

Federated Learning over Wireless Device-to-Device Networks: Algorithms and Convergence Analysis

Hong Xing, Osvaldo Simeone, and Suzhi Bi

Abstract

The proliferation of Internet-of-Things (IoT) devices and cloud-computing applications over siloed data centers is motivating renewed interest in the collaborative training of a shared model by multiple individual clients via federated learning (FL). To improve the communication efficiency of FL implementations in wireless systems, recent works have proposed compression and dimension reduction mechanisms, along with digital and analog transmission schemes that account for channel noise, fading, and interference. This prior art has mainly focused on star topologies consisting of distributed clients and a central server. In contrast, this paper studies FL over wireless device-to-device (D2D) networks by providing theoretical insights into the performance of digital and analog implementations of decentralized stochastic gradient descent (DSGD). First, we introduce generic digital and analog wireless implementations of communication-efficient DSGD algorithms, leveraging random linear coding (RLC) for compression and over-the-air computation (AirComp) for simultaneous analog transmissions. Next, under the assumptions of convexity and connectivity, we provide convergence bounds for both implementations. The results demonstrate the dependence of the optimality gap on the connectivity and on the signal-to-noise ratio (SNR) levels in the network. The analysis is corroborated by experiments on an image-classification task.

Index Terms

Federated learning, distributed learning, decentralized stochastic gradient descent, over-the-air computation, D2D networks.

Part of this paper has been presented at the IEEE International Workshop on Signal Processing Advances in Wireless Communications (SPAWC), May 2020 [1].

H. Xing and S. Bi are with the College of Electronic and Information Engineering, Shenzhen University, Shenzhen, 518060, China (e-mails: hong.xing, bsz@szu.edu.cn).

O. Simeone is with the King's Communications, Learning, and Information Processing (KCLIP) lab, Department of Engineering, King's College London, London, WC2R 2LS, U.K. (e-mail: osvaldo.simeone@kcl.ac.uk).

The work of O. Simeone is supported by the European Research Council under the European Union's Horizon 2020 research and innovation program under grant 725731.

I. INTRODUCTION

With the proliferation of Internet-of-Things (IoT) devices and cloud-computing applications over siloed data centres, *distributed learning* has become a critical enabler for artificial intelligence (AI) solutions [2], [3]. In distributed learning, multiple agents collaboratively train a machine learning model via the exchange of training data, model parameters and/or gradient vectors over geographically distributed computing resources and data. *Federated learning (FL)* refers to distributed learning protocols that do not directly exchange the training data in an attempt to reduce the communication load and to limit privacy concerns [4]–[7]. In conventional FL, multiple clients train a shared model by exchanging model-related parameters with a central node. This class of protocols hence relies on a parameter-server architecture, which is typically realized in wireless settings via a base station-centric network topology [8]–[13].

There are important scenarios in which a base station-centric architecture is either unavailable or undesirable due to coverage, privacy, implementation efficiency, or fault-tolerance considerations [14], [15]. In such cases, distributed learning must rely on a peer-to-peer, edge-based, communication topology that encompasses device-to-device (D2D) links among individual learning agents over an arbitrary connectivity graph. With the exception of [1], [16], all prior works on decentralized FL nevertheless assume either ideal or rate-limited but *noiseless* D2D communications. This paper is the first to offer a rigorous convergence analysis of digital and analog implementations of wireless D2D FL, with the aim for providing insights on the effect of wireless impairments caused by link blockages, pathloss, channel fading, and interference.

A. Related Work

The problem of alleviating the communication load in FL systems has been widely investigated, mostly under the assumption of noiseless, rate-limited links, and *star topologies*. Key elements of these solutions are compression and dimension-reduction operations that map the original model parameters or gradient vectors into representations defined by a limited number of bits and/or sparsity. Important classes of solutions include unbiased compressors (e.g., [8]–[10]) and biased compressors with error-feedback mechanisms (e.g., [11]–[13]).

In a *D2D architecture*, even in the presence of noiseless communication, devices can only exchange information with their respective neighbors, making consensus mechanisms essential to ensure agreement towards the common learning goal [17], [18]. A well-known protocol integrating stochastic gradient (SGD) and consensus is *Decentralized Stochastic Gradient Descent*

(DSGD), which has been further extended and improved via gradient tracking [19], as well as via variance-reduction schemes for large data heterogeneity among agents [20]. Similar to FL in star topologies, the communication overhead in decentralized learning can be reduced via compression, as demonstrated by the CHOCO-SGD algorithm [21], [22]. The protocol, combining DSGD with biased compression, was studied for strongly convex and smooth objectives in [21] and for non-convex smooth objectives in [22]. It was further combined with event-triggered protocols in [23].

A large number of recent works have proposed communication strategies and multi-access protocols for *FL in wireless star topologies* [24]–[28]. At the physical layer, *over-the-air computation* (AirComp) was investigated in [13], [25], [29]–[32] as a promising solution to support simultaneous transmissions by leveraging the waveform superposition property of the wireless medium. Unlike conventional digital communication over orthogonal transmission blocks, AirComp is based on analog, e.g., uncoded, transmission, which enables the estimate of aggregated statistics directly from the received baseband samples. This reduces the communication burden, relieving the network from the need to decode individual information separately for all participating devices. The impact of AirComp on the performance of FL was studied in [31], [32]. The authors in [31] proposed an adaptive learning-rate scheduler and investigated the convergence of the resulting protocol. Reference [32] derived sufficient conditions in terms of signal-to-noise ratio (SNR) for the FL algorithm to attain the same convergence rate as in the ideal noiseless case.

The literature on *decentralized FL in wireless D2D architecture* is, in contrast, still quite limited. A DSGD based algorithm termed MATCHA was proposed in [33] by accounting for interference among nearby links. Adopting a general interference graph, the scheme was based on sampling a matching decomposition of the graph, whereby the connectivity-critical links are activated with a higher probability. By relying on a matching decomposition, MATCHA schedules noiseless non-interfering communication links in parallel. No attempt was made to leverage non-orthogonal physical layer protocols such as AirComp. In contrast, in the conference version [1] of this paper, wireless protocols for both digital and analog implementations of error-compensated DSGD were designed by including AirComp. However, no theoretical analysis was offered on the convergence of the considered wireless decentralized FL algorithms.

B. Main Contributions

In this paper, we provide for the first time a rigorous analysis of digital and analog transmission protocols tailored to FL over wireless D2D networks in terms of their convergence properties. The contributions of this paper are specifically summarized as follows.

- 1) We introduce generic digital and analog wireless implementations of DSGD algorithms. The protocols rely on compression via *random linear coding (RLC)* as applied to model differential information. The general protocols enable broadcasting for digital transmission; and both broadcasting and AirComp for analog transmission.
- 2) Under the assumptions of convexity and connectivity, we derive *convergence bounds* for the generic digital wireless implementation. The result demonstrates the dependence of the optimality gap on the connectivity of the graph and on the model differential estimation error due to compression.
- 3) We also provide convergence bounds for the analog wireless implementation. The analysis reveals the impact of topology and channel noise, as well as the importance of implementing an *adaptive consensus step size*. To the best of our knowledge, this is the first time that an adaptive consensus step size is shown to be beneficial for convergence.
- 4) We provide numerical experiments for image classification, confirming the benefits of the proposed adaptive consensus rate, and demonstrating the agreement between analytical and empirical results.

The remainder of this paper is organized as follows. The system model is presented in Section [II](#). Digital and analog transmission protocols are introduced in Section [III](#). The convergence analysis for both implementations is presented in Section [IV](#) and Section [V](#), respectively. Numerical performance results are described in Section [VI](#), followed by conclusions in Section [VII](#).

C. Notations

We use the upper case boldface letters for matrices and lower case boldface letters for vectors. We also use $\|\cdot\|$ to denote the Euclidean norm of a vector or the spectral norm of a matrix, and $\|\cdot\|_F$ to denote the Frobenius norm of a matrix. The average of vectors \mathbf{x}_i over $i \in \mathcal{V}$ is defined as $\bar{\mathbf{x}} = \frac{1}{K} \sum_{i \in \mathcal{V}} \mathbf{x}_i$. Notations $\text{Tr}(\cdot)$ and $(\cdot)^T$ denote the trace and the transpose of a matrix, respectively. $\mathbb{E}[\cdot]$ stands for the statistical expectation of a random variable. \mathbf{I} represents an identity matrix with appropriate size, and \triangleq indicates a mathematical definition. $\lambda_i(\cdot)$ denotes the i th largest eigenvalue of a matrix.

II. SYSTEM MODEL

In this paper, we consider a FL problem in a decentralized setting as shown in Fig. 1, in which a set $\mathcal{V} = \{1, \dots, K\}$ of K devices can only communicate with their respective neighbors over a wireless D2D network whose connectivity is characterized by an undirected graph $\mathcal{G}(\mathcal{V}, \mathcal{E})$, with \mathcal{V} denoting the set of nodes and $\mathcal{E} \subseteq \{(i, j) \in \mathcal{V} \times \mathcal{V} \mid i \neq j\}$ the set of edges. The set of neighbors of node i is denoted as $\mathcal{N}_i = \{j \in \mathcal{V} \mid (i, j) \in \mathcal{E}\}$. Following the FL framework, each device has available a local data set, and all devices collaboratively train a machine learning model by exchanging model-related information without directly disclosing data samples to one another.

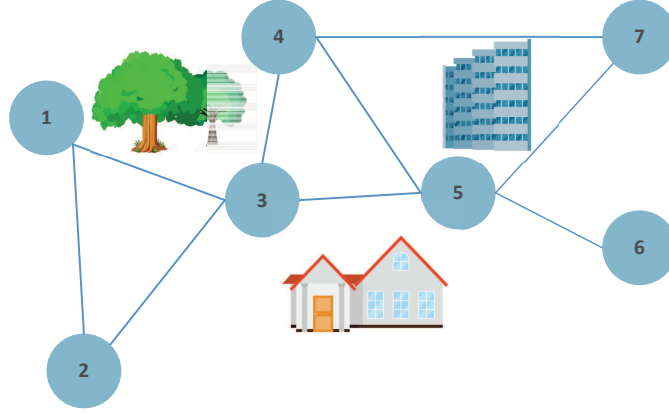


Fig. 1. The connectivity graph $\mathcal{G}(\mathcal{V}, \mathcal{E})$ for a wireless D2D network.

A. Learning Model

Each device $i \in \mathcal{V}$ has access to its local data set \mathcal{D}_i , which may have non-empty intersection with the data set \mathcal{D}_j of any other device $j \in \mathcal{V}$, $i \neq j$. All devices share a common machine learning model class, which is parametrized by a vector $\boldsymbol{\theta} \in \mathbb{R}^{d \times 1}$. As a typical example, the model class may consist of a neural network with a given architecture. The goal of the network is to solve the empirical risk minimization problem [19], [22]

$$(P0) : \underset{\boldsymbol{\theta}}{\text{Minimize}} \quad F(\boldsymbol{\theta}) \triangleq \frac{1}{K} \sum_{i \in \mathcal{V}} f_i(\boldsymbol{\theta}),$$

where $f_i(\boldsymbol{\theta}) = \frac{1}{|\mathcal{D}_i|} \sum_{\boldsymbol{\xi} \in \mathcal{D}_i} l(\boldsymbol{\theta}, \boldsymbol{\xi})$ is the local empirical risk function for device i with $l(\boldsymbol{\theta}; \boldsymbol{\xi})$ denoting the loss accruing from parameter $\boldsymbol{\theta}$ on data sample $\boldsymbol{\xi} \in \mathcal{D}_i$, which may include the effect of regularization.

To enable decentralized learning, we adopt CHOCO-SGD, a communication-efficient variant of DSGD [21]. At the start of each iteration $t + 1$, device $i \in \mathcal{V}$ has in its memory its current model iterate $\boldsymbol{\theta}_i^{(t)}$, the corresponding estimated version $\hat{\boldsymbol{\theta}}_i^{(t)}$ and the estimated iterates $\hat{\boldsymbol{\theta}}_j^{(t)}$ for all its neighbors $j \in \mathcal{N}_i$. We note that an equivalent version of the algorithm that requires less memory can be found in [21, Algorithm 6], but we do not consider it here since it does not change the communication requirements. Furthermore, at each iteration t , device $i \in \mathcal{V}$ first executes a local update step by SGD based on its data set \mathcal{D}_i as

$$\boldsymbol{\theta}_i^{(t+1/2)} = \boldsymbol{\theta}_i^{(t)} - \eta^{(t)} \hat{\nabla} f_i(\boldsymbol{\theta}_i^{(t)}), \quad (1)$$

where $\eta^{(t)}$ denotes the learning rate, and $\hat{\nabla} f_i(\boldsymbol{\theta}_i^{(t)})$ is an estimate of the exact gradient $\nabla f_i(\boldsymbol{\theta}_i^{(t)})$ obtained from a mini-batch $\mathcal{D}_i^{(t)} \subseteq \mathcal{D}_i$ of the data set, i.e., $\hat{\nabla} f_i(\boldsymbol{\theta}_i^{(t)}) = \frac{1}{|\mathcal{D}_i^{(t)}|} \sum_{\boldsymbol{\xi} \in \mathcal{D}_i^{(t)}} \nabla l(\boldsymbol{\theta}_i^{(t)}; \boldsymbol{\xi})$.

Then, each device $i \in \mathcal{V}$ compresses the difference $\boldsymbol{\theta}_i^{(t+1/2)} - \hat{\boldsymbol{\theta}}_i^{(t)}$ between the locally updated model (1) and the previously estimated iterate $\hat{\boldsymbol{\theta}}_i^{(t)}$. The compressed difference $\mathcal{C}^{(t)}(\boldsymbol{\theta}_i^{(t+1/2)} - \hat{\boldsymbol{\theta}}_i^{(t)})$ is then exchanged with the neighbors of node i . Assuming that communication is reliable — an assumption that we will revisit in the rest of the paper. Each device $i \in \mathcal{V}$ updates the estimated model parameters $\hat{\boldsymbol{\theta}}_j^{(t)}$ for itself and for its neighbors as

$$\hat{\boldsymbol{\theta}}_j^{(t+1)} = \hat{\boldsymbol{\theta}}_j^{(t)} + \mathcal{D}^{(t)} \left(\mathcal{C}^{(t)}(\boldsymbol{\theta}_j^{(t+1/2)} - \hat{\boldsymbol{\theta}}_j^{(t)}) \right), \quad j \in \{i\} \cup \mathcal{N}_i, \quad (2)$$

where $\mathcal{D}^{(t)}(\cdot)$ is a decoding function. Next, device $i \in \mathcal{V}$ executes a consensus update step by correcting the updated model (1) using the estimated parameters (2) as

$$\boldsymbol{\theta}_i^{(t+1)} = \boldsymbol{\theta}_i^{(t+1/2)} + \zeta^{(t)} \sum_{j \in \mathcal{N}_i \cup \{i\}} w_{ij} \left(\hat{\boldsymbol{\theta}}_j^{(t+1)} - \hat{\boldsymbol{\theta}}_i^{(t+1)} \right), \quad (3)$$

where $\zeta^{(t)}$ is the consensus rate, and the mixing matrix $\mathbf{W} = \mathbf{W}^T \in \mathbb{R}^{K \times K}$ is selected to be *doubly stochastic*, i.e., $[\mathbf{W}]_{ij} = w_{ij} \geq 0$, $\mathbf{W}\mathbf{1} = \mathbf{1}$, $\mathbf{1}^T \mathbf{W} = \mathbf{1}^T$ and $\|\mathbf{W} - \mathbf{1}\mathbf{1}^T/K\|_2 < 1$. A typical choice is to set $w_{ij} = \alpha$ for all $j \in \mathcal{N}_i$, $w_{ii} = 1 - |\mathcal{N}_i|\alpha$, and $w_{ij} = 0$ otherwise, where constant $\alpha > 0$ is a design parameter. We postpone discussion regarding the compression operator $\mathcal{C}^{(t)}(\cdot)$ and the decoding operator $\mathcal{D}^{(t)}(\cdot)$ to Section II-C. The considered decentralized learning protocol is summarized in Algorithm 1.

Finally, we make the following assumptions that are widely adopted in the literature on decentralized stochastic optimization [21].

Algorithm 1: Decentralized Learning with Noiseless Communication

Input : Consensus step size $\zeta^{(t)}$, SGD learning step size $\eta^{(t)}$, connectivity graph $\mathcal{G}(\mathcal{V}, \mathcal{E})$ and mixing matrix \mathbf{W}

1 Initialize at each node $i \in \mathcal{V}$: $\boldsymbol{\theta}_i^{(0)}, \hat{\boldsymbol{\theta}}_j^{(0)} = \mathbf{0}$, $\forall j \in \mathcal{N}_i \cup \{i\}$;

2 **for** $t = 0, 1, \dots, T-1$ **do**

3 **for** each device $i \in \mathcal{V}$ **do** in parallel

4 update $\boldsymbol{\theta}_i^{(t+1/2)} = \boldsymbol{\theta}_i^{(t)} - \eta^{(t)} \hat{\nabla} f_i(\boldsymbol{\theta}_i^{(t)})$;

5 compress the difference $\boldsymbol{\theta}_i^{(t+1/2)} - \hat{\boldsymbol{\theta}}_i^{(t)}$ to obtain $\mathcal{C}^{(t)}(\boldsymbol{\theta}_i^{(t+1/2)} - \hat{\boldsymbol{\theta}}_i^{(t)})$;

6 **for** each neighboring device $j \in \mathcal{N}_i$ **do** in parallel

7 send $\mathcal{C}^{(t)}(\boldsymbol{\theta}_i^{(t+1/2)} - \hat{\boldsymbol{\theta}}_i^{(t)})$;

8 receive $\mathcal{C}^{(t)}(\boldsymbol{\theta}_j^{(t+1/2)} - \hat{\boldsymbol{\theta}}_j^{(t)})$;

9 **end**

10 update $\hat{\boldsymbol{\theta}}_j^{(t+1)} = \hat{\boldsymbol{\theta}}_j^{(t)} + \mathcal{D}^{(t)} \left(\mathcal{C}^{(t)}(\boldsymbol{\theta}_j^{(t+1/2)} - \hat{\boldsymbol{\theta}}_j^{(t)}) \right)$, for $j \in \{i\} \cup \mathcal{N}_i$;

11 update $\boldsymbol{\theta}_i^{(t+1)} = \boldsymbol{\theta}_i^{(t+1/2)} + \zeta^{(t)} \sum_{j \in \mathcal{N}_i \cup \{i\}} w_{ij} \left(\hat{\boldsymbol{\theta}}_j^{(t+1)} - \hat{\boldsymbol{\theta}}_i^{(t+1)} \right)$.

12 **end**

13 **end**

Output: $\boldsymbol{\theta}_i^{(T-1)}$, $\forall i \in \mathcal{V}$

Assumption 2.1: Each local empirical risk function $f_i(\boldsymbol{\theta})$, $i \in \mathcal{V}$, is L -smooth and μ -strongly convex, that is, for all $\boldsymbol{\theta}_1 \in \mathbb{R}^{d \times 1}$ and $\boldsymbol{\theta}_2 \in \mathbb{R}^{d \times 1}$, it satisfies the inequalities

$$f_i(\boldsymbol{\theta}_1) \leq f_i(\boldsymbol{\theta}_2) + \nabla f_i(\boldsymbol{\theta}_2)^T (\boldsymbol{\theta}_1 - \boldsymbol{\theta}_2) + \frac{L}{2} \|\boldsymbol{\theta}_1 - \boldsymbol{\theta}_2\|^2, \quad (4)$$

and

$$f_i(\boldsymbol{\theta}_1) \geq f_i(\boldsymbol{\theta}_2) + \nabla f_i(\boldsymbol{\theta}_2)^T (\boldsymbol{\theta}_1 - \boldsymbol{\theta}_2) + \frac{\mu}{2} \|\boldsymbol{\theta}_1 - \boldsymbol{\theta}_2\|^2. \quad (5)$$

Assumption 2.2: The variance of the mini-batch gradient $\hat{\nabla} f_i(\boldsymbol{\theta}_i)$ is bounded as

$$\mathbb{E}_{\mathcal{D}_i^{(t)}} [\|\hat{\nabla} f_i(\boldsymbol{\theta}_i) - \nabla f_i(\boldsymbol{\theta}_i)\|^2] \leq \sigma_i^2, \quad (6)$$

and its expected Euclidean norm is bounded as

$$\mathbb{E}_{\mathcal{D}_i^{(t)}} [\|\hat{\nabla} f_i(\boldsymbol{\theta}_i)\|^2] \leq G^2, \quad (7)$$

where the expectation $\mathbb{E}_{\mathcal{D}_i^{(t)}} [\cdot]$ is taken over the selection of a mini-batch $\mathcal{D}_i^{(t)} \subseteq \mathcal{D}_i$.

B. Communication Model

As seen in Fig. 2, at the end of every iteration t , communication takes place within one communication block of a total number N of channel uses spanning over M equal-length slots, denoted by $\mathcal{S} = \{1, \dots, M\}$. Slow fading remains constant across all iterations, and is binary, determining whether a link is blocked or not. A link $(i, j) \in \mathcal{E}$ is by definition not *blocked*, while all the other links $(i, j) \notin \mathcal{E}$ are blocked. We assume that the connectivity graph $\mathcal{G}(\mathcal{V}, \mathcal{E})$ with all the unblocked links as edges satisfies the following assumption.

Assumption 2.3: Graph $\mathcal{G}(\mathcal{V}, \mathcal{E})$ is a connected graph.

For all unblocked links $(i, j) \in \mathcal{E}$, the channel coefficient between device i and j is modelled as

$$h'_{ij}^{(t)} \triangleq \sqrt{A_0} \left(\frac{d_{ij}}{d_0} \right)^{-\frac{\gamma}{2}} h_{ij}^{(t)}, \quad (8)$$

where the fast fading coefficient $h_{ij}^{(t)} \sim \mathcal{CN}(0, 1)$ remains unchanged within one communication block and varies independently across blocks, and the path loss gain $\sqrt{A_0}(d_0/d_{ij})^{\gamma/2}$ is constant across all iterations, where A_0 is the average channel power gain at reference distance d_0 ; d_{ij} is the distance between device i and j ; and γ is the path loss exponent factor.

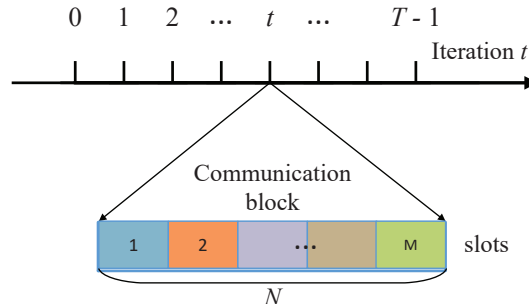


Fig. 2. Timeline of training iterations and communication blocks: A communication block of N channel uses, divided into M slots, is employed to exchange the compressed difference between model parameters among neighboring devices.

Each device is subject to an energy constraint of $NP^{(t)}$ per communication block. If a device is active for $M' \leq M$ slots, the energy per symbol is hence given by $\frac{NP^{(t)}}{M'N/M} = P^{(t)}\frac{M}{M'}$. The mean-square power of the added white Gaussian noise (AWGN) is denoted as N_0 .

C. Compression

In this subsection, we describe the assumed compression operator $\mathcal{C}(\cdot)$ and decompression operator $\mathcal{D}(\cdot)$ that are used in the update (3). We specifically adopt *random linear coding (RLC)* compression [10]. Let $\mathbf{A}^{(t)} = \frac{1}{\sqrt{m}} \mathbf{H} \mathbf{R}^{(t)}$ be the linear encoding matrix, where $\mathbf{H} \in \{\pm 1\}^{m \times d}$

with $m \leq d$ is a partial Hadamard matrix with mutually orthogonal rows, i.e., $\frac{1}{d}\mathbf{H}\mathbf{H}^T = \mathbf{I}$; and $\mathbf{R}^{(t)} \in \mathbb{R}^{d \times d}$ is a diagonal matrix with its diagonal entries $[\mathbf{R}^{(t)}]_{ii} \triangleq r_i^{(t)}$ drawn from uniform distributions such that $\Pr(r_i^{(t)} = 1) = \Pr(r_i^{(t)} = -1) = 0.5$, for all $i = 1, \dots, d$. The compression operator is given by the linear projection $\mathcal{C}^{(t)}(\mathbf{u}) = \mathbf{A}^{(t)}\mathbf{u}$, while decoding takes place as $\mathcal{D}^{(t)}(\mathbf{v}) = \frac{m}{d}(\mathbf{A}^{(t)})^T\mathbf{v}$. The concatenation of the compression and decompression operators, namely, $\mathcal{D}^{(t)}(\mathcal{C}^{(t)}(\mathbf{u})) = \frac{m}{d}(\mathbf{A}^{(t)})^T\mathbf{A}^{(t)}\mathbf{u}$, satisfies the *compression operator* [10], [21]

$$\mathbb{E} \left\| \mathbf{u} - \frac{m}{d}(\mathbf{A}^{(t)})^T\mathbf{A}^{(t)}\mathbf{u} \right\|^2 = \left(1 - \frac{m}{d}\right) \|\mathbf{u}\|^2, \text{ for all } \mathbf{u} \in \mathbb{R}^{d \times 1}. \quad (9)$$

We note that the random matrices $\{\mathbf{R}^{(t)}\}$ need to be shared among devices prior to the start of the communication protocol such that the same random sequence $\{\mathbf{A}^{(t)}\}$ is agreed upon by all devices.

III. DIGITAL AND ANALOG TRANSMISSION PROTOCOLS

In this section, we describe digital and analog wireless implementations of the decentralized learning algorithm reviewed in the previous section. The implementations are meant to serve as prototypical templates for the deployment of decentralized learning. In practice, specific protocols are in need to specify the scheduling strategy used to allocate slots in Fig. 2 to devices. The analysis in this paper, to be detailed in Section IV and Section V, applies to any scheduling algorithm.

A. Digital Transmission

In digital transmission protocol, devices represent their model updates as digital messages for transmission. The number $B_i^{(t)}$ of bits that device $i \in \mathcal{V}$ can successfully broadcast to its neighbors during a slot allocated to it by the scheduling algorithm is limited by the neighboring device with the worst channel power gain. Accordingly, we have

$$B_i^{(t)} = \frac{N}{M} \log_2 \left(1 + \frac{P^{(t)}}{N_0} M \min_{j \in \mathcal{N}_i} |h_{ij}^{(t)}|^2 \right). \quad (10)$$

We recall that, in (10), the number M of time slots per iteration is decided by the scheduling scheme.

To quantize the encoded vector $\mathbf{A}_i^{(t)}(\theta_i^{(t+1/2)} - \hat{\theta}_i^{(t)}) \in \mathbb{R}^{m \times 1}$ into $B_i^{(t)}$ bits, we employ a simple per-element b -bit quantizer $\mathcal{Q}_b(\cdot)$ with chip-level precision so that $b = 64$ or $b = 32$ is for double-precision or single-precision floating-point, respectively, according to IEEE 754

standard. Communication constraints thus impose the inequality $bm_i^{(t)} \leq B_i^{(t)}$, which is satisfied by setting $m_i^{(t)} = \lfloor B_i^{(t)}/b \rfloor$. Based on the (received) quantized signal, each device $i \in \mathcal{V}$ updates the estimated model parameters of its own as well as of its neighbors in $j \in \{i\} \cup \mathcal{N}_i$ as (cf. (2))

$$\hat{\boldsymbol{\theta}}_j^{(t+1)} = \hat{\boldsymbol{\theta}}_j^{(t)} + \frac{m_j^{(t)}}{d} (\mathbf{A}_j^{(t)})^T \mathcal{Q}_b \left(\mathbf{A}_j^{(t)} (\boldsymbol{\theta}_j^{(t+1/2)} - \hat{\boldsymbol{\theta}}_j^{(t)}) \right). \quad (11)$$

In order to implement update (11), each node $j \in \mathcal{V}$ and its neighbors in set \mathcal{N}_j can share *a priori* a common sequence of (pseudo-)random matrix $\tilde{\mathbf{A}}_j^{(t)} \in \mathbb{R}^{m \times d}$ satisfying the assumption described in Section II-C. If node j sends its current value $m_j^{(t)}$ to all neighbors and if $m_j^{(t)} \leq m$, all nodes can thus select the same submatrix $\mathbf{A}_j^{(t)}$ from $\tilde{\mathbf{A}}_j^{(t)}$ to evaluate (11). The described digital implementation is summarized in Algorithm 2 in Appendices.

B. Analog Transmission

With analog transmission, devices directly transmit their respective updated parameters by mapping analog signals to channel uses, without the need for digitization. As studied in [25], [30], in addition to broadcast as in digital transmission, it is also useful to schedule all devices that share a common neighbor for simultaneous transmission in order to enable AirComp. The considered class of protocols can accommodate any scheduling scheme that, as in [1], operates over pairs of consecutive time slots in order to leverage AirComp. In the first slot of each pair, one or more center nodes receive a superposition of the signals simultaneously transmitted by all their respective neighbors. In the second slot, the center nodes serve as broadcast transmitters communicating to all their neighbors. The total number M of time slots is thus given by twice as the number n of pairs of time slots, which is specified by the scheduling policy in use.

To elaborate on the operation of analog transmission protocol, we will use the following notation. For each device $i \in \mathcal{V}$, we define a set $\mathcal{S}_i^{\text{Tx}} \subseteq \mathcal{S}$ of transmission slots, with $\mathcal{S}_i^{\text{Tx}} = \mathcal{S}_i^{\text{BT}} \cup \mathcal{S}_i^{\text{AT}}$ partitioned into disjoint subsets $\mathcal{S}_i^{\text{BT}}$ and $\mathcal{S}_i^{\text{AT}}$ ($\mathcal{S}_i^{\text{BT}} \cap \mathcal{S}_i^{\text{AT}} = \emptyset$). Subset $\mathcal{S}_i^{\text{BT}}$ denotes the set of transmission slots in which device i broadcasts to its neighbors, and $\mathcal{S}_i^{\text{AT}}$ denotes the set of slots in which device i transmits to enable AirComp. Similarly, we define the set $\mathcal{S}_i^{\text{Rx}} \subseteq \mathcal{S}$ of receiving slots for device i as $\mathcal{S}_i^{\text{Rx}} = \mathcal{S}_i^{\text{BR}} \cup \mathcal{S}_i^{\text{AR}}$ with $\mathcal{S}_i^{\text{BR}} \cap \mathcal{S}_i^{\text{AR}} = \emptyset$, where $\mathcal{S}_i^{\text{BR}}$ and $\mathcal{S}_i^{\text{AR}}$ denote the sets of receiving slots in which device $i \in \mathcal{V}$ receives from a transmitter in broadcast and AirComp modes, respectively. Fig. III-B serves as an example illustrating the above definitions.

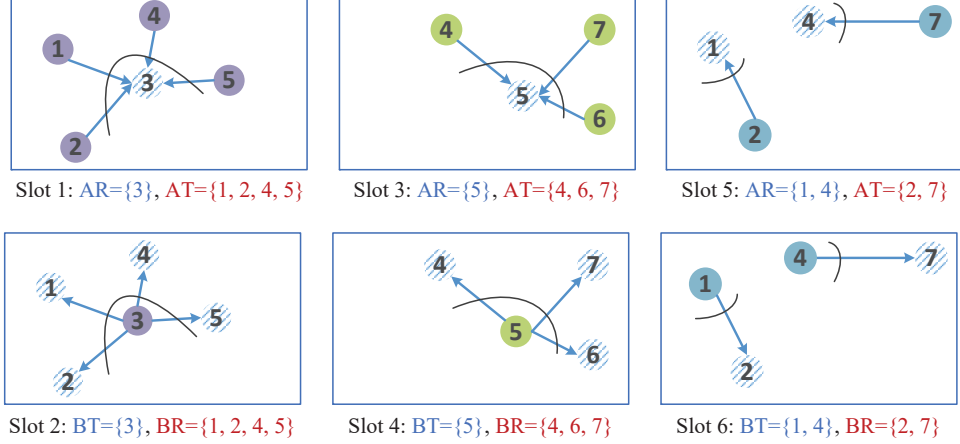


Fig. 3. An example illustrates pairs of consecutive time slots for analog transmissions given a scheduling scheme that yields $M = 6$ for the connectivity graph shown in Fig. 1. There are following non-empty sets for each node: $\mathcal{S}_1^{\text{AT}} = \{1\}$, $\mathcal{S}_1^{\text{BT}} = \{6\}$, $\mathcal{S}_1^{\text{AR}} = \{5\}$, $\mathcal{S}_1^{\text{BR}} = \{2\}$; $\mathcal{S}_2^{\text{AT}} = \{1, 5\}$, $\mathcal{S}_2^{\text{BT}} = \{2, 6\}$; $\mathcal{S}_3^{\text{BT}} = \{2\}$, $\mathcal{S}_3^{\text{AR}} = \{1\}$; $\mathcal{S}_4^{\text{AT}} = \{1, 3\}$, $\mathcal{S}_4^{\text{BT}} = \{6\}$, $\mathcal{S}_4^{\text{AR}} = \{5\}$, $\mathcal{S}_4^{\text{BR}} = \{2, 4\}$; $\mathcal{S}_5^{\text{AT}} = \{1\}$, $\mathcal{S}_5^{\text{BT}} = \{4\}$, $\mathcal{S}_5^{\text{AR}} = \{3\}$, $\mathcal{S}_5^{\text{BR}} = \{2\}$; $\mathcal{S}_6^{\text{AT}} = \{3\}$, $\mathcal{S}_6^{\text{BT}} = \{4\}$; and $\mathcal{S}_7^{\text{AT}} = \{3, 5\}$, $\mathcal{S}_7^{\text{BR}} = \{4, 6\}$.

We now describe the transmitted and the received signals in each pair of slots of the communication protocol.

Odd slots: All devices $i \in \mathcal{V}$ operating in AirComp mode for a center node j in an odd slot $s \in \mathcal{S}_i^{\text{AT}} \cap \mathcal{S}_j^{\text{AR}}$ concurrently transmit the signals

$$\mathbf{x}_{ij}^{(t,s)} = \frac{\sqrt{\gamma_j^{(t,s)}}}{h_{ij}^{(t)}} w_{ji} \mathbf{A}^{(t)} (\boldsymbol{\theta}_i^{(t+1/2)} - \hat{\boldsymbol{\theta}}_i^{(t)}), \quad (12)$$

where $\gamma_j^{(t,s)}$ is a power scaling factor for channel alignment at device j . The receiving center node, device j obtains

$$\mathbf{y}_j^{(t,s)} = \sqrt{\gamma_j^{(t,s)}} \sum_{i \in \mathcal{N}_j^{(s)}} w_{ji} \mathbf{A}^{(t)} (\boldsymbol{\theta}_i^{(t+1/2)} - \hat{\boldsymbol{\theta}}_i^{(t)}) + \mathbf{n}_j^{(t,s)}, \quad (13)$$

where $\mathcal{N}_j^{(s)}$ is the neighboring set of device j operating in AirComp at slot s , and $\mathbf{n}_j^{(t,s)} \sim \mathcal{CN}(\mathbf{0}, N_0 \mathbf{I})$ is the received AWGN at slot s of iteration t . Device j estimates the *combined* model parameters $\sum_{i \in \mathcal{N}_j^{(s)}} w_{ji} (\boldsymbol{\theta}_i^{(t+1/2)} - \hat{\boldsymbol{\theta}}_i^{(t)})$ via the linear estimator

$$\hat{\mathbf{y}}_j^{(t,s)} = \frac{m}{d} (\mathbf{A}^{(t)})^T \Re \left\{ \mathbf{y}_j^{(t,s)} / \sqrt{\gamma_j^{(t,s)}} \right\}. \quad (14)$$

Even slots: Any device $i \in \mathcal{V}$ operating in broadcast mode in an even slot $s \in \mathcal{S}_i^{\text{BT}}$ transmits a signal

$$\mathbf{x}_i^{(t,s)} = \sqrt{\alpha_i^{(t,s)}} \mathbf{A}^{(t)} (\boldsymbol{\theta}_i^{(t+1/2)} - \hat{\boldsymbol{\theta}}_i^{(t)}), \quad (15)$$

where $\alpha_i^{(t,s)}$ is device i 's transmitting power scaling factor in slot $s \in \mathcal{S}_i^{\text{BT}}$ of iteration t . Each neighboring device $j \in \mathcal{N}_i^{(s)}$, with $s \in \mathcal{S}_j^{\text{BR}}$, receives from device i the signal

$$\mathbf{y}_{ij}^{(t,s)} = \sqrt{\alpha_i^{(t,s)}} h_{ij}^{(t)} \mathbf{A}^{(t)} (\boldsymbol{\theta}_i^{(t+1/2)} - \hat{\boldsymbol{\theta}}_i^{(t)}) + \mathbf{n}_j^{(t,s)}, \quad (16)$$

where $\mathbf{n}_j^{(t,s)} \sim \mathcal{CN}(\mathbf{0}, N_0 \mathbf{I})$ is the received AWGN. Device j estimates the signal $\boldsymbol{\theta}_i^{(t+1/2)} - \hat{\boldsymbol{\theta}}_i^{(t)}$ via the linear estimator

$$\hat{\mathbf{y}}_{ij}^{(t,s)} = w_{ji} \frac{m}{d} (\mathbf{A}^{(t)})^T \Re \left\{ \frac{\mathbf{y}_{ij}^{(t,s)}}{\sqrt{\alpha_i^{(t,s)} h_{ij}^{(t)}}} \right\}, \quad (17)$$

where $\Re\{\cdot\}$ denotes the real part of its argument.

Next, device $j \in \mathcal{V}$ updates its estimate of the combined model parameters from all neighboring devices in \mathcal{N}_j by aggregating the estimates obtained at all receiving slots in set $\mathcal{S}_j^{\text{Rx}} = \mathcal{S}_j^{\text{BR}} \cup \mathcal{S}_j^{\text{AR}}$ as

$$\hat{\mathbf{y}}_j^{(t+1)} = \hat{\mathbf{y}}_j^{(t)} + \sum_{s \in \mathcal{S}_j^{\text{AR}}} \hat{\mathbf{y}}_j^{(t,s)} + \sum_{s \in \mathcal{S}_j^{\text{BR}}} \hat{\mathbf{y}}_{isj}^{(t,s)}, \quad (18)$$

where node $i_s \in \mathcal{N}_j$ is the node that transmits in broadcast mode in slot $s \in \mathcal{S}_j^{\text{BR}}$. The initial estimate of the combined model parameters is given by $\hat{\mathbf{y}}_i^{(0)} = \mathbf{0}$, $\forall i \in \mathcal{V}$.

The power scaling parameters $\gamma_j^{(t,s)}$ (cf. (12)) and $\alpha_i^{(t,s)}$ (cf. (15)) for $s \in \mathcal{S}_i^{\text{Tx}}$ need to be properly chosen such that the power consumed by device $i \in \mathcal{V}$ per communication block satisfies

$$\sum_{s \in \mathcal{S}_i^{\text{AT}}} \mathbb{E}[\|\mathbf{x}_{ij_s}^{(t,s)}\|^2] + \sum_{s \in \mathcal{S}_i^{\text{BT}}} \mathbb{E}[\|\mathbf{x}_i^{(t,s)}\|^2] \leq NP^{(t)}, \quad \forall i \in \mathcal{V}, \quad (19)$$

where node j_s is the center node connected to node i in slot $s \in \mathcal{S}_i^{\text{AT}}$. Applying a simple equal power policy across different transmission slots of a device $i \in \mathcal{V}$ for all communication blocks, we have (cf. (19))

$$\mathbb{E}[\|\mathbf{x}_{ij}^{(t,s)}\|^2] \leq NP^{(t)} / |\mathcal{S}_i^{\text{Tx}}|, \quad \forall s \in \mathcal{S}_i^{\text{AT}}, \quad (20)$$

$$\mathbb{E}[\|\mathbf{x}_i^{(t,s)}\|^2] \leq NP^{(t)} / |\mathcal{S}_i^{\text{Tx}}|, \quad \forall s \in \mathcal{S}_i^{\text{BT}}. \quad (21)$$

In addition, device $j \in \mathcal{V}$ needs to update the estimate of its own model parameter $\hat{\boldsymbol{\theta}}_j^{(t+1)}$ as

$$\hat{\boldsymbol{\theta}}_j^{(t+1)} = \hat{\boldsymbol{\theta}}_j^{(t)} + \frac{m}{d} (\mathbf{A}^{(t)})^T \mathbf{A}^{(t)} (\boldsymbol{\theta}_j^{(t+1/2)} - \hat{\boldsymbol{\theta}}_j^{(t)}). \quad (22)$$

Finally, device $j \in \mathcal{V}$ approximates update (3) as

$$\boldsymbol{\theta}_j^{(t+1)} = \boldsymbol{\theta}_j^{(t+1/2)} + \zeta^{(t)} \left(w_{jj} \hat{\boldsymbol{\theta}}_j^{(t+1)} + \hat{\mathbf{y}}_j^{(t+1)} - \hat{\boldsymbol{\theta}}_j^{(t+1)} \right). \quad (23)$$

To sum up, the proposed analog implementation is presented in Algorithm 3 in Appendices.

IV. CONVERGENCE ANALYSIS FOR DIGITAL TRANSMISSION

In this section, we derive convergence properties of the general class of digital transmission protocols presented in Section III-A. The analysis holds for any fixed transmission schedule, which determines the number M of slots. We start by recalling that, at each iteration t , update (11) is carried out by device $i \in \mathcal{V}$ for all nodes $j \in \{i\} \cup \mathcal{N}_i$. In (11), the concatenation of compression, quantization, and decompression yields an output vector $\frac{m_j^{(t)}}{d}(\mathbf{A}_j^{(t)})^T \mathcal{Q}_b(\mathbf{A}_j^{(t)} \mathbf{u}_j^{(t)})$ for the input vector $\mathbf{u}_j^{(t)} = \boldsymbol{\theta}_j^{(t+1/2)} - \hat{\boldsymbol{\theta}}_j^{(t)}$. The number $m_j^{(t)} = \lfloor B_j^{(t)}/b \rfloor$ of rows of matrix $\mathbf{A}_j^{(t)}$ at iteration t depends on the current rate (10) supported by the fast fading channels between device j and its neighbors. Taking the randomness of the fading realizations into account, the counterpart of the compression operator (9) under digital transmission is given by the following lemma.

Lemma 4.1: On average over RLC and fading channels, the mean-square estimation error for the concatenation of compression, quantization, and decompression under digital transmission satisfies

$$\mathbb{E} \left\| \mathbf{u} - \frac{m_i^{(t)}}{d}(\mathbf{A}_i^{(t)})^T \mathcal{Q}_b(\mathbf{A}_i^{(t)} \mathbf{u}) \right\|^2 \leq (1 - \omega^{(t)}) \|\mathbf{u}\|^2, \quad (24)$$

for all $\mathbf{u} \in \mathbb{R}^{d \times 1}$ and for all $i \in \mathcal{V}$, with $\omega^{(t)} = \min_{i \in \mathcal{V}} \omega_i^{(t)}$, where we have $\omega_i^{(t)} = \frac{1}{d} + \frac{1}{d} \sum_{n=2}^d G_i^{(t)}(n)$ with the function $G_i^{(t)}(n): \mathbb{Z}_+ \mapsto \mathbb{R}$, $i \in \mathcal{V}$, defined as

$$G_i^{(t)}(n) = \exp \left(-\frac{N_0}{P^{(t)}} \frac{1}{MA_0} \left(2^{nb\frac{M}{N}} - 1 \right) \sum_{j \in \mathcal{N}_i} \left(\frac{d_{ij}}{d_0} \right)^r \right). \quad (25)$$

Proof: Please refer to Appendix C. ■

By (24), the parameter $\omega = \min_{t \in \{0, \dots, T-1\}} \omega^{(t)} \in [0, 1]$ is a measure of the quality of the reconstruction of the model difference used in update (11). Supposing static channel conditions in which the transmission rate (10) remains constant over iterations, we have $m_i^{(t)} = m_i, \forall i \in \mathcal{V}$. In these conditions, the right-hand side (RHS) of (24) can reduce to $(1 - \frac{m_i}{d}) \|\mathbf{u}\|^2$ (see Appendix C), which is exactly the RHS of (9) given $m = m_i$ and $\mathbf{A}^{(t)} = \mathbf{A}_i^{(t)}$. Note that $\omega^{(t)}$ is increasing with $P^{(t)}$. In particular, when the transmission power $P^{(t)} \rightarrow \infty$, it is seen in (25) that $G_i(n) \rightarrow 1$, thus leading to zero mean-square estimation error ($\omega^{(t)} \rightarrow 1$).

With Lemma 4.1, the convergence properties of the digital protocol can be quantified in a manner similar to [21, Theorem 4]. To this end, we define the following topology-related parameters dependent on the mixing matrix \mathbf{W} : the spectral gap $\delta = 1 - \|\frac{\mathbf{1}\mathbf{1}^T}{K} - \mathbf{W}\|$; the

parameter $\beta = \|\mathbf{I} - \mathbf{W}\|_2$; and the function $p(\delta, \omega) = \frac{\delta^2 \omega}{2(16\delta + \delta^2 + 4\beta^2 + 2\delta\beta^2 - 8\delta\omega)}$ that depends on the spectral gap δ and on the model-difference estimation quality $\omega = \min_{t \in \{0, T-1\}} \{\omega^{(t)}\}$. Then, the convergence of the digital implementation is provided by the following theorem.

Theorem 4.1 (Optimality Gap for Digital Transmission [21, Theorem 19]): For learning rate $\eta^{(t)} = \frac{3.25}{\mu} \frac{1}{t+a}$ with $a \geq \max\{\frac{5}{p(\delta, \omega)}, \frac{13L}{\mu}\}$, and consensus step size $\zeta^{(t)} = \frac{2p(\delta, \omega)}{\delta} \triangleq \zeta_0(\delta, \omega)$, on average over RLC and fading channels $\{h_{ij}^{(t)}\}$, Algorithm 2 yields an optimality gap satisfying

$$\begin{aligned} \mathbb{E}[F(\tilde{\boldsymbol{\theta}}_T)] - F^* &\leq \mathbb{E} \left[\frac{1}{S_T} \sum_{t=0}^{T-1} w^{(t)} F(\bar{\boldsymbol{\theta}}^{(t)}) \right] - F^* \\ &\leq \underbrace{\frac{\mu}{3.25} \frac{a^3 - 3.25a^2}{S_T} v_e^{(0)}}_{\text{centralized error}} + \underbrace{\frac{1.625(2a+T)T\bar{\sigma}^2}{\mu S_T} \frac{K}{K}}_{\text{consensus error}} + \underbrace{\frac{158.45 \times 24LT}{\mu^2(p(\delta, \omega))^2 S_T} G^2}, \end{aligned} \quad (26)$$

where $w^{(t)} = (a+t)^2$; $S_T = \sum_{t=0}^{T-1} w^{(t)}$; $\tilde{\boldsymbol{\theta}}_T = \frac{1}{S_T} \sum_{t=0}^{T-1} w^{(t)} \bar{\boldsymbol{\theta}}^{(t)}$ is the weighted sum of the average iterate $\bar{\boldsymbol{\theta}}^{(t)} = \frac{1}{K} \sum_{i \in \mathcal{V}} \boldsymbol{\theta}_i^{(t)}$ across all the communication rounds; F^* denotes the optimum objective value for problem (P0); μ is the parameter for μ -strongly convex function $F(\boldsymbol{\theta})$; $v_e^{(0)} = \|\bar{\boldsymbol{\theta}}^{(0)} - \boldsymbol{\theta}^*\|^2$ measures the initial distance to the optimal model parameter; and $\bar{\sigma}^2 = \frac{1}{K} \sum_{i \in \mathcal{V}} \sigma_i^2$ is the average of the mini-batch gradient variance over all devices.

Remark 4.1: The labels “centralized error” and “consensus error” in (26) refer to decomposition of the upper bound on optimality gap into a term that accounts for the performance of the average model $\bar{\boldsymbol{\theta}}^{(t)} = \frac{1}{K} \sum_{i \in \mathcal{V}} \boldsymbol{\theta}_i^{(t)}$ — the “centralized error”, and a term that measures the disagreement among agents — the “consensus error”. To gain insights into how wireless resources, channel conditions, and topology of the connectivity graph affect the performance of the digital wireless implementation, we can rewrite (26) using relevant parameters in “big O” notation as [21, Theorem 4]

$$\mathbb{E}[F(\tilde{\boldsymbol{\theta}}_T)] - F^* \leq \mathcal{O}\left(\frac{\bar{\sigma}^2}{\mu KT}\right) + \mathcal{O}\left(\frac{\bar{\sigma}^2}{\mu KT^2} + \frac{LG^2}{\mu^2(p(\delta, \omega))^2 T^2}\right) + \mathcal{O}\left(\frac{\mu}{T^3}\right). \quad (27)$$

This result shows that when the total number of iterations T is sufficiently large, the optimality gap (27) behaves as $\mathcal{O}\left(\frac{\bar{\sigma}^2}{\mu KT}\right)$, which recovers the convergence rate of centralized SGD with ideal communications. However, when the wireless communication resources are limited, and hence $NT \ll \infty$, the second term, scaling as $\mathcal{O}\left(\frac{1}{T^2}\right)$, becomes equally important in (27), demonstrating the impact of the topology via δ and β , as well as the effect of the quality of digital transmission via ω . Since the function $p(\delta, \omega)$ is monotonically increasing with $\delta \in [0, 1]$ and $\omega \in [0, 1]$, the second term in (27) decreases with δ and ω . This implies that convergence is

improved for more connected graphs with larger δ [34], and for smaller estimation errors with larger ω .

A. Numerical Illustration

In this subsection, we corroborate the analysis by numerically evaluating each constituent term in the upper bounds (26) on the optimality gap. We consider a setup consisting of $K = 20$ devices that are located at randomly and independently selected distances in the interval [50, 200] m away from a center position, with all angles (in radius) uniformly distributed in the interval $[0, 2\pi]$. The connectivity graph, accounting for the impact of slow fading, is modelled as: (i) a complete graph; (ii) a planar 5×4 grid graph; (iii) a planar 5×4 grid graph with torus wrapping; or (iv) a star graph as in conventional FL. We set the strong-convexity parameter as $\mu = 0.0002$, and the smoothness factor as $L = 0.16$. We plot the upper bound at iteration t normalized by the corresponding value at $t = 0$, hence evaluating the improvement in the expected optimality gap. The SNR is defined as the received SNR, averaged over fast fading, at a distance of 125 meters (m) away from the deployment center. Other parameters are set as $d_0 = 1$ m, $A_0 = 10^{-3.35}$, $\gamma = 3.76$, $N_0 = -169$ dBm and $\alpha = 2/(\lambda_1(\mathbf{L}) + \lambda_{K-1}(\mathbf{L}))$, where \mathbf{L} is the Laplacian of the connectivity graph.

We apply the vertex coloring-based scheduling proposed in [1] in order to determine the number of slots. Fig. 4 plots separately the centralized and the consensus errors, as well as the overall error in (26), for different number of iterations $t = 2000$ and $t = 5000$ under a planar topology with torus wrapping. The centralized error does not depend on the SNR, and it decreases at the fastest rate over iterations. The consensus error decreases with the received SNR due to the improvement in the parameter ω that characterizes the quality of model reconstruction (cf. (26)). As a result, the consensus error dominates the optimality gap until the received SNR level increases to a sufficiently large value dependent on the iteration t . Furthermore, the overall optimality gap approaches the centralized error as the SNR increases.

We now turn to an analysis of the impact of the topology of the connectivity graph on the convergence for digital transmission. To this end, we set the same received SNR for all devices ignoring the impact of pathloss in order to isolate the impact of different topologies. We employ TDMA-based scheduling that assigns only one device as the transmitter at one slot such that there are equal number $M = K$ of slots for all topologies. Fig. 5 reports the optimality gap, along with the constituent errors in (26). The optimality gap decreases with the spectral gap δ of

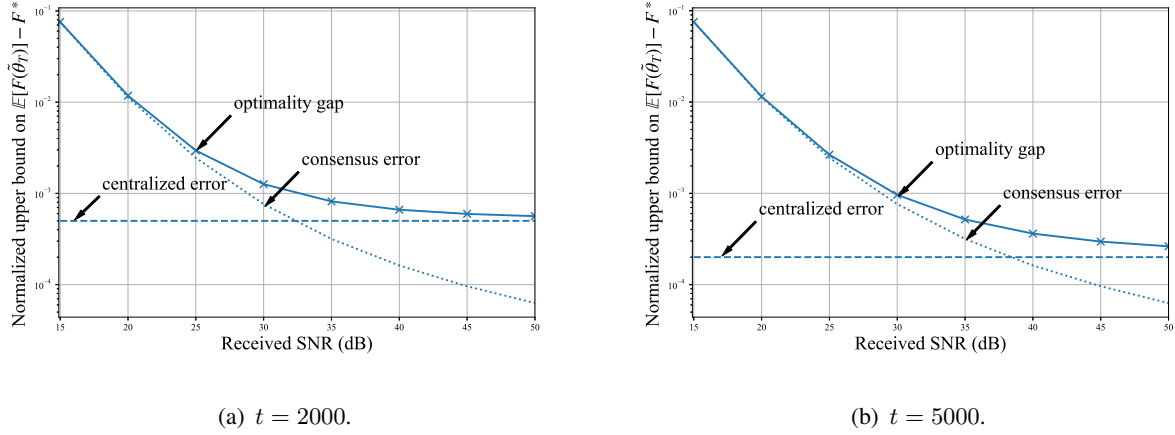


Fig. 4. Normalized upper bounds (26) on the optimality gap versus the received SNR levels for a planar grid graph with torus wrapping and $N = 10^4$ ($a = 4 \times 10^7$).

the connectivity graph, which equals $\delta = 1, 0.31, 0.103$, and 0.095 , for complete graph, planar graph with and without torus wrapping, and star topology, respectively. Fig. 5 shows that the consensus error contributes very little to the overall error for densely connected graphs, such as the complete graph and the planar grid with torus wrapping, while it becomes dominant in less densely connected graphs, such as the planar grid and the star graph.

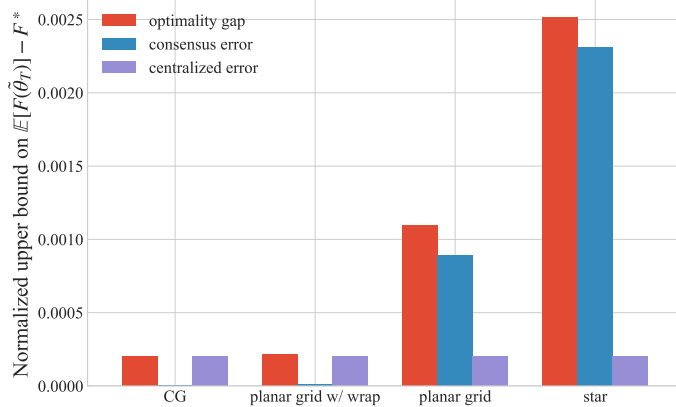


Fig. 5. Normalized upper bounds (26) on the optimality gap for different topologies of the connectivity graph with $M = K$, $\text{SNR} = 30$ dB, and $N = 10^4$ for $t = 5000$ ($a = 1.3 \times 10^8$).

V. CONVERGENCE ANALYSIS FOR ANALOG TRANSMISSION

In this section, we derive convergence properties for the general class of analog transmission schemes described in Section III-B. The analysis holds for any fixed scheduling scheme operating

in pairs of slots as described in Section III-B. We start by noting that, while for the digital implementation, the number $m_j^{(t)} = \lfloor B_j^{(t)}/b \rfloor$ rows of matrix $\mathbf{A}_j^{(t)}$ for device $j \in \mathcal{V}$ depends on the fast fading channels between device j and its neighbors, for the analog implementation, the number m of rows of matrix $\mathbf{A}^{(t)}$ is fixed as the number $m = N/M$ of available channel uses in each slot of the communication block. Therefore, for analog communication, we can directly use (9) to quantify the quality of the estimate of the model difference used in update (22). However, due to the presence of channel noise, update (18) for the combined parameters of neighboring devices does not satisfy $\bar{\boldsymbol{\theta}}^{(t+1)} = \bar{\boldsymbol{\theta}}^{(t+1/2)}$. This calls for a novel derivation of convergence properties that does not follow from [21, Theorem 19].

Next, we relate the update in (23), which is subject to Gaussian noise, to the noiseless update in (3) in the following lemma.

Lemma 5.1: The consensus update (23) for analog implementation is equivalent to

$$\boldsymbol{\theta}_i^{(t+1)} = \boldsymbol{\theta}_i^{(t+1/2)} + \zeta^{(t)} \sum_{j \in \mathcal{N}_i \cup \{i\}} w_{ij} \left(\hat{\boldsymbol{\theta}}_j^{(t+1)} - \hat{\boldsymbol{\theta}}_i^{(t+1)} \right) + \zeta^{(t)} \sum_{\tau=0}^t \frac{m}{d} (\mathbf{A}^{(\tau)})^T \tilde{\mathbf{n}}_i^{(\tau)}, \quad (28)$$

where $\tilde{\mathbf{n}}_i^{(t)} \sim \mathcal{N}(0, \tilde{N}_{0i}^{(t)} \mathbf{I})$ is the effective noise with power

$$\tilde{N}_{0i}^{(t)} = \frac{1}{2} \frac{N_0}{NP^{(t)}} \left(\sum_{s \in \mathcal{S}_i^{\text{AR}}} \max_{j \in \mathcal{N}_i^{(s)}} \left\{ |\mathcal{S}_j| w_{ij}^2 \frac{\|\mathbf{u}_j^{(t)}\|^2}{|h_{ij}^{(t)}|^2} \right\} + \sum_{s \in \mathcal{S}_i^{\text{BR}}} |\mathcal{S}_{js}| w_{ij_s}^2 \frac{\|\mathbf{u}_{js}^{(t)}\|^2}{|h_{ij_s}^{(t)}|^2} \right), \quad (29)$$

where we denoted $\mathbf{u}_j^{(t)} = \boldsymbol{\theta}_j^{(t+1/2)} - \hat{\boldsymbol{\theta}}_j^{(t)}$.

Proof: Please refer to Appendix D. ■

Comparing (28) with (3) reveals that consensus updates (23) for analog implementation are noisy approximation of those for ideal communication used by Algorithm 1 and digital implementation used by Algorithm 2. Note, in particular, that by (28), unlike Algorithms 1-2, we no longer have the preservation of the average of the model parameters across the network. In fact, the average $\bar{\boldsymbol{\theta}}^{(t+1)} = 1/K \sum_{i \in \mathcal{V}} \boldsymbol{\theta}_i^{(t+1)}$ of the model parameters, obtained by averaging over $i \in \mathcal{V}$ on both sides of (28), is corrupted by Gaussian noise as

$$\bar{\boldsymbol{\theta}}^{(t+1)} = \bar{\boldsymbol{\theta}}^{(t+1/2)} + \zeta^{(t)} \frac{1}{K} \sum_{i \in \mathcal{V}} \sum_{\tau=0}^t \frac{m}{d} (\mathbf{A}^{(\tau)})^T \tilde{\mathbf{n}}_i^{(\tau)}. \quad (30)$$

Next, we investigate how the noisy consensus updates given by (28) affect the convergence of Algorithm 3. In the proof of Theorem 19 in [21, Appendix D], the key step leading to the

final convergence result is to construct an error sequence defined as

$$e^{(t)} = \underbrace{\sum_{i \in \mathcal{V}} \mathbb{E} \|\bar{\theta}^{(t)} - \theta_i^{(t)}\|^2}_{\text{consensus error}} + \underbrace{\sum_{i \in \mathcal{V}} \mathbb{E} \|\hat{\theta}_i^{(t+1)} - \theta_i^{(t+1/2)}\|^2}_{\text{compression error}}, \quad (31)$$

where the first term measures the consensus error, while the second term accounts for the impact of compression. It is shown in [21, Appendix D] that the above two sub-terms are coupled with each other via a recursive relation that yields the main result summarized in the previous section. However, as discussed, their approach cannot be directly applied to analog transmission due to the fact that the consensus preserving property no longer holds, i.e., $\bar{\theta}^{(t+1)} \neq \bar{\theta}^{(t+1/2)}$, as seen from (30). To address this challenge, we need a new upper bound on (31). To this end, we first introduce the function

$$p^{(t)}(\delta, \omega) = \min\{\tilde{p}^{(t)}(\delta, \omega), p(\delta, \omega)\}, \quad (32)$$

where

$$\tilde{p}^{(t)}(\delta, \omega) = \frac{\delta \zeta_0(\delta, \omega)}{\sqrt[4]{\tilde{N}_{0,T} t / a' + 1}} - \left(\frac{\delta^2}{4} + \frac{2}{\omega} \beta^2 \right) \frac{(\zeta_0(\delta, \omega))^2}{\left(\sqrt[4]{\tilde{N}_{0,T} t / a' + 1} \right)^2}, \quad (33)$$

with $p(\delta, \omega)$ and $\zeta_0(\delta, \omega)$ defined in Theorem 4.1. We also denote

$$\tilde{N}_{0,T} = \max_{t \in \{0, \dots, T-1\}} \left\{ \sum_{i \in \mathcal{V}} \tilde{N}_{0i}^{(t)} \right\}, \quad (34)$$

and $\omega = m/d$. We will see that the function $p^{(t)}(\delta, \omega)$ plays an analogous role to $p(\delta, \omega)$ for digital transmission in that it contributes to the decaying rate of the error sequence defined in (31). Specifically, both $\tilde{p}^{(t)}(\delta, \omega)$ and $p(\delta, \omega)$ are increasing functions of δ and ω .

A key ingredient of the proposed approach is to design a consensus step size that is adaptive to the iteration index t . This is because a consensus step size $\zeta^{(t)} = \zeta_0$, as used in [21], [22] for ideal communication, causes the accumulated channel noise term in (30) to grow with t , leading to a possible divergence of the upper bound on $e^{(t)}$ (see (68) in [21, Appendix] for details). To suppress the error growth induced by channel noise, we propose an adaptive consensus step size $\zeta^{(t)} = \frac{\zeta_0(\delta, \omega)}{\sqrt[4]{\tilde{N}_{0,T} t / a' + 1}}$, based on which we have the following lemma.

Lemma 5.2: For learning rate $\eta^{(t)} = \frac{3.25}{\mu} \frac{1}{t+a}$ with $a \geq \max\{\frac{5}{p^{(t)}(\delta, \omega)}, \frac{13L}{\mu}\}$, adaptive consensus step size $\zeta^{(t)} = \frac{\zeta_0(\delta, \omega)}{\sqrt[4]{\tilde{N}_{0,T} t / a' + 1}}$ with $a' > a \sqrt[4]{\tilde{N}_{0,T}}$, and $T < \infty$, on average over RLC, the error sequence in (31) satisfies

$$e^{(t+1)} \leq \left(1 - \frac{p^{(t)}(\delta, \omega)}{2} \right) e^{(t)} + \frac{1}{p^{(t)}(\delta, \omega)} (\eta^{(t)})^2 \left(24KG^2 + A(\delta, \omega) \sqrt[4]{\tilde{N}_0} \right), \quad (35)$$

where $A(\delta, \omega) = \delta(\zeta_0(\delta, \omega)a')^3(2 - \omega)\omega^2d(\frac{\mu}{3.25})^2$ is a function depending on the spectral gap δ of graph $\mathcal{G}(\mathcal{V}, \mathcal{E})$ and the estimation quality ω .

Proof: Please refer to Appendix E. ■

Remark 5.1: When communication is ideal, i.e., $\tilde{N}_{0,T} \rightarrow 0$, the function $p^{(t)}(\delta, \omega)$ reduces to $p(\delta, \omega)$, and the upper bound (35) reduces to the result derived in [21, Lemma 21].

By leveraging Lemma 5.2, the convergence of the analog implementation scheme is revealed as follows.

Theorem 5.1 (Optimality Gap for Analog Transmission): For a given total number T of iterations, learning rate $\eta^{(t)} = \frac{3.25}{\mu} \frac{1}{t+a}$ with $a \geq \max\{\frac{5}{p^{(t)}(\delta, \omega)}, \frac{13L}{\mu}\}$, and adaptive consensus step size $\zeta^{(t)} = \frac{\zeta_0(\delta, \omega)}{\sqrt[4]{\tilde{N}_{0,T}t/a'+1}}$ with $a' > a\sqrt[4]{\tilde{N}_{0,T}}$, on average over RLC, channel noise and conditioned on the fading realizations $\{h_{ij}^{(t)}\}$, Algorithm 3 yields an optimality gap satisfying

$$\mathbb{E}[F(\tilde{\boldsymbol{\theta}}_T)] - F^* \leq \mathbb{E} \left[\frac{1}{S_T} \sum_{t=0}^{T-1} w_t F(\bar{\boldsymbol{\theta}}^{(t)}) \right] - F^* \leq \underbrace{\frac{\mu}{3.25} \frac{a^3 - 3.25a^2}{S_T} v_e^{(0)} + \frac{1.625(2a+T)T}{\mu S_T} \bar{\sigma}^2}{\text{centralized error}} + \underbrace{\frac{158.45 \times 24G^2 LT}{\mu^2 (p^{(T)}(\delta, \omega))^2 S_T} + \frac{158.45 \frac{A(\delta, \omega)}{K} \sqrt[4]{\tilde{N}_{0,T}} LT}{\mu^2 (p^{(T)}(\delta, \omega))^2 S_T} + \frac{1}{K^2} D(\delta, \omega) \sqrt{\tilde{N}_{0,T}}}_{\text{noiseless consensus error AWGN error}}, \quad (36)$$

where $D(\delta, \omega) = \omega^2 d \frac{\mu}{3.25} (\zeta_0(\delta, \omega)a')^2$.

Proof: Please refer to Appendix F. ■

Remark 5.2: Similar to analysis given in Section IV, we decompose the upper bound on the optimality gap (36) into different terms. The ‘‘centralized error’’ carries the same meaning as that in (26); the ‘‘noiseless consensus error’’ quantifies the disagreement among agents in the absence of communication noise, i.e., $\tilde{N}_{0i}^{(t)} = 0$ (cf. (29)); and the ‘‘AWGN error’’ accounts for the impact of Gaussian noise on the consensus updates in (23). To gain insights into how wireless resources, channel conditions, and topology of the connectivity graph affect the performance of the analog wireless implementation, we can write (36) in the following form

$$\mathbb{E}[F(\tilde{\boldsymbol{\theta}}_T)] - F^* \leq \mathcal{O} \left(\frac{\sqrt{\tilde{N}_{0,T}}}{K^2} \right) + \mathcal{O} \left(\frac{\bar{\sigma}^2}{\mu K T^2} + \frac{\left(24G^2 + \frac{A(\delta, \omega)}{K} \sqrt[4]{\tilde{N}_{0,T}} \right) L}{\mu^2 (p^{(T)}(\delta, \omega))^2 T^2} \right) + \mathcal{O} \left(\frac{\bar{\sigma}^2}{\mu K T} \right) + \mathcal{O} \left(\frac{\mu}{T^3} \right). \quad (37)$$

Compared with (27), the upper bound (37) reveals that, even if $T \rightarrow \infty$, there is a non-vanishing term $\mathcal{O} \left(\frac{\sqrt{\tilde{N}_{0,T}}}{K^2} \right)$, as well as a term scaling as $\mathcal{O} \left(\frac{\sqrt[4]{\tilde{N}_{0,T}}}{(p^{(T)}(\delta, \omega))^2 T^2} \right)$ that may not vanish either. We

also note that $\tilde{N}_{0,T}$ is non-decreasing with T by its definition (34). This highlights the significant impact of the topology parameters δ and β , as well as of the quality of the reconstruction $\omega = m/d$ via function $p^{(T)}(\delta, \omega)$. Furthermore, as the effective noise power $\tilde{N}_{0i}^{(t)}$ in (29) for $i \in \mathcal{V}$ decreases with the transmitting power $P^{(t)}$, the convergence rate improves with $P^{(t)}$. In particular, when $P^{(t)} \rightarrow \infty$, we have $\tilde{N}_{0,T} = 0$, and therefore (37) reduces exactly to the corresponding expression for the noiseless case in (27).

A. Numerical Illustration

In this subsection, we elaborate on the results obtained from the analysis above by following the approach in Section IV-A. For the scheduling scheme, we apply the vertex coloring-based strategy proposed in [1]. Fig. 6 plots the upper bounds and the individual terms in (36) as in Fig. 4 for digital communication under the planar grid topology with torus wrapping. The centralized error and the noiseless consensus error are independent of SNR. Note that the latter depends on the parameter $\omega = \frac{N/M}{d}$ that quantifies the quality of the estimate in (9), which is independent of the SNR. As a result, the impact of SNR on the optimality gap is only through the AWGN error, which dominates the other terms when the SNR level is sufficiently small, here around 25 dB, while it becomes negligible when the SNR is large enough, here larger than 40 dB.

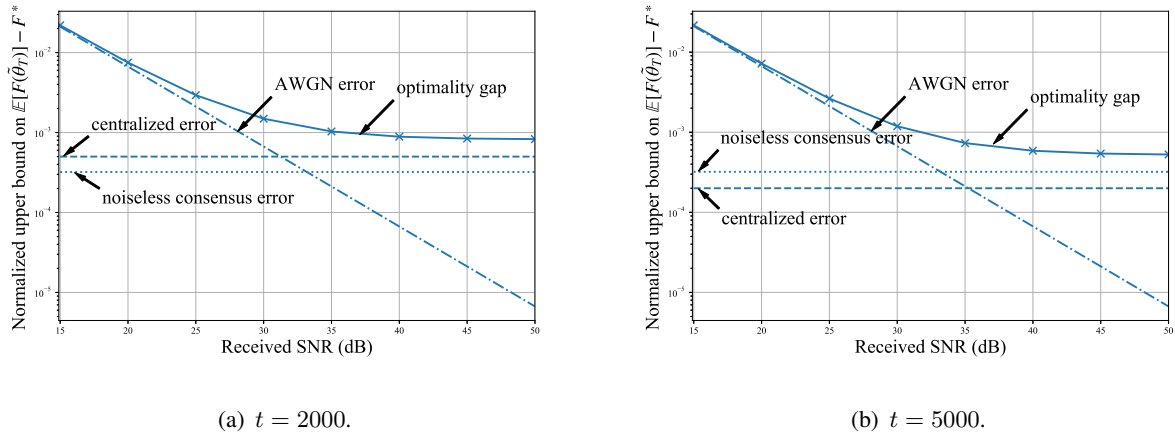


Fig. 6. Normalized upper bounds (36) on the optimality gap versus the received SNR levels for a planar grid graph with torus wrapping and $N = 10^4$ ($a = 7 \times 10^6$, $a' = a \sqrt[4]{\tilde{N}_{0,T}}$, and $\tilde{N}_{0,T} = 10^{-5}$).

Next, we study the impact of the topology of the connectivity graph on the convergence for analog transmission in Fig. 7. The general conclusions are analogous to Fig. 5, which illustrates the corresponding results for digital communication. In particular, the noiseless consensus error

is shown to increase when the connectivity graph is less densely connected, i.e., with smaller δ . In contrast, the AWGN error is less sensitive to a change in connectivity, and it becomes dominant for sufficiently large number of iterations such as $t = 5000$.

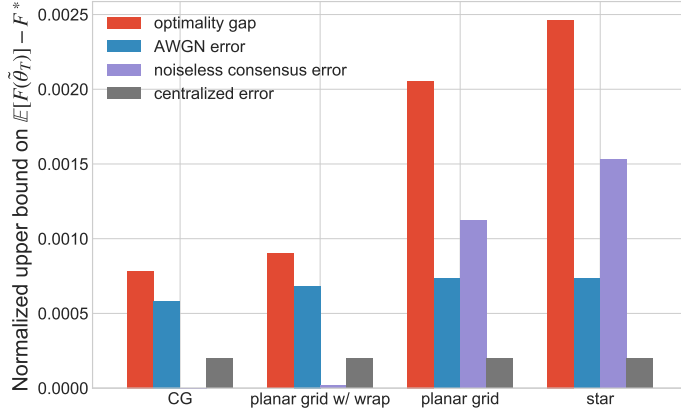


Fig. 7. Normalized upper bounds (36) on the optimality gap for different topologies of the connectivity graph with $M = K$, SNR = 30 dB, and $N = 10^4$ for $t = 5000$ ($a = 3 \times 10^7$, $a' = 2a\sqrt[4]{\tilde{N}_{0,T}}$, and $\tilde{N}_{0,T} = 10^{-5}$ corresponding to 30 dB received SNR).

VI. NUMERICAL EXPERIMENTS

In this section, we corroborate the analysis developed in Sections IV and V by evaluating the empirical performance of the digital and analog wireless implementations over a wireless D2D network. We consider the learning task of image classification over the Fashion-MNIST dataset [35] that consists of 28×28 images divided into $C = 10$ classes. There are 60,000 training data samples and 10,000 test data samples, which are equally divided among classes. Each device $i \in \mathcal{V}$ has data samples from at least six different classes, with the number of missing classes being uniformly selected in the set $\{0, 1, 2, 3, 4\}$. An equal number x_i of data samples are then selected across the available classes at device i , such that the total number $\sum_{i \in \mathcal{V}} \sum_{n=1}^{10} \mathbb{1}_{n,i} x_i$ of training samples in use are maximized, where $\mathbb{1}_{n,i}$ is an indicator function denoting whether class $n \in \{1, \dots, 10\}$ is available at device i ($\mathbb{1}_{n,i} = 1$) or not ($\mathbb{1}_{n,i} = 0$). All devices share a softmax regression model. We adopt the standard cross-entropy loss with ℓ_2 regularization $f_i(\boldsymbol{\theta}) = -\frac{1}{|\mathcal{D}_i|} \sum_{\boldsymbol{\xi} \in \mathcal{D}_i} \sum_{n \in \Omega_i} y_{i,n} \log(\text{softmax}_n(\mathbf{a}_i(\boldsymbol{\theta}, \boldsymbol{\xi}))) + \frac{\mu}{2} \|\boldsymbol{\theta}\|^2$, where Ω_i denotes the set of available classes on device $i \in \mathcal{V}$; $y_{i,n} \in \{0, 1\}$ is the one-hot encoded label corresponding to the n th class for data sample $\boldsymbol{\xi} \in \mathcal{D}_i$; the n th entry of softmax is defined

as $\text{softmax}_n(\mathbf{z}) = \frac{e^{z_n}}{\sum_{n=1}^C e^{z_n}}$, where $\mathbf{z} = (z_1, \dots, z_C)^T$; and $\mathbf{a}_i(\boldsymbol{\theta}, \boldsymbol{\xi})$ is the vector consisting of the logits for device i with its n th entry corresponding to class n . The SGD is executed with mini-batch size of $|\mathcal{D}_i^{(t)}| = 64$, and we add momentum to all updates with a factor of 0.9. In line with the local empirical risk function defined above, the strong-convexity parameter is set as $\mu = 0.002$. The smoothness factor L is numerically computed as the largest eigenvalue of the data Gramian matrix.

We adopt the vertex coloring-based scheduling schemes used in [1]. The optimal value F^* used for quantifying the empirical optimality gap is numerically obtained by the standard decentralized SGD (applying Algorithm 1 with $\mathcal{C} = \mathcal{D} = \mathbf{I}$ for sufficiently large T), with the hyper parameters $b > 0$ and $c > 0$ for the learning rate $\eta^{(t)} = \frac{b}{t+c}$, as well as the (constant) consensus step size ζ_0 , optimized via grid search. We consider $K = 20$ devices with the connectivity graph modelled as a planar 5×4 grid graph with torus wrapping or a chain graph. All the other parameters for simulations are set as in Section IV-A unless specified otherwise. As benchmarks, we consider decentralized learning with ideal communications, i.e., applying Algorithm 1 with $\mathcal{C}^{(t)} = \mathcal{D}^{(t)} = \mathbf{I}$, as well as independent learning that carries out training based solely on local data with no communications among devices.

We start by studying the impact of the proposed adaptive consensus rate on the convergence for analog transmission. We recall that the analysis in Section V has revealed that a consensus rate $\zeta^{(t)} = \frac{\zeta_0}{t/1000+1}$ is necessary in order to ensure convergence. In line with the analysis, Fig. 8 shows that the optimality gap with fixed consensus rates diverges as a function of the number of iteration t , while it converges with the proposed adaptive consensus rate. The figure also demonstrates the advantages brought by communications with respect to (w.r.t) local training with no communications.

Next, we provide a performance comparison between digital and analog wireless implementations in terms of the analytical and the empirical upper bounds on the optimality gap. We plot the optimality gap normalized by its value evaluated at iteration $t = 200$ and $t = 0$ for the analytical and the empirical results, respectively. For the empirical results, we set $\eta^{(t)} = \frac{3.25}{\mu} \frac{1}{t+200}$ for all schemes; $\zeta^{(t)} = 0.001$ for the schemes of ideal, digital and no communication; and $\zeta^{(t)} = \frac{0.001}{t/d+1}$ with $d = 35355, 42045, 50000, 62872$, and 74767 for $N = 500, 1000, 2000, 5000$, and 10000 , respectively, for the analog implementation. Fig. 9 compares digital and analog implementations, benchmarked by ideal communication and no communication. The analytical bounds shown in Fig. 9(a) are in general agreement with the empirical results shown in Fig. 9(b), demonstrating

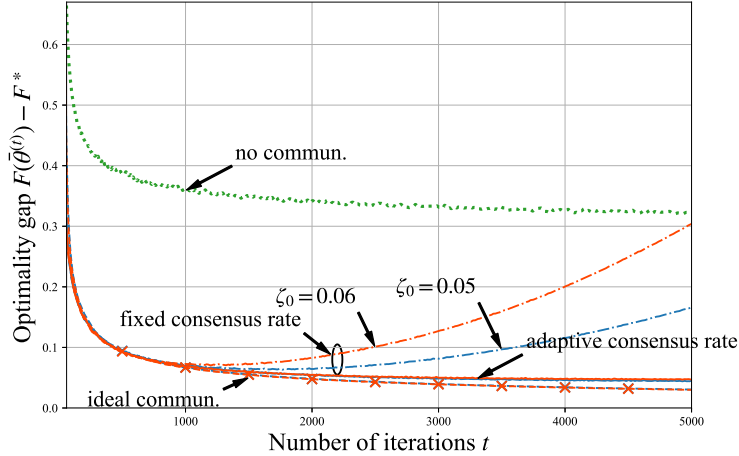
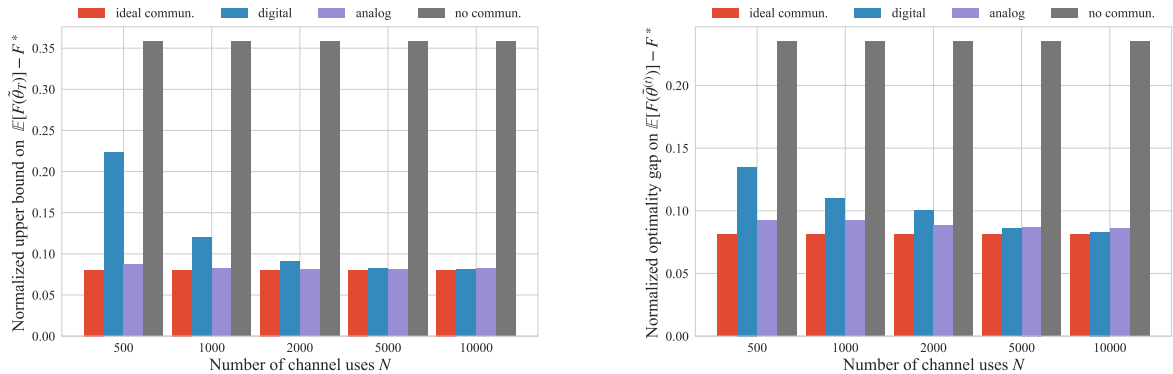


Fig. 8. Empirical optimality gap versus the number of iterations t for analog transmission over a planar grid graph with torus wrapping, with SNR = 30 dB and $N = 8000$ ($a = 200$).

the practical relevance of the theory developed in this paper. In particular, the analysis correctly predicts the advantages of the analog implementation for sufficiently small number of channel uses N , and the marginal benefits of the digital implementation in the complementary regime of a large number of channel uses, e.g., when we have $N \geq 5000$.



(a) Normalized upper bounds on the optimality gap for different schemes. (b) Normalized empirical optimality gap for different schemes.

Fig. 9. Performance comparison of analog and digital implementations in terms of normalized (upper bounds on) optimality gap for iteration $t = 2500$ for different number N of channel uses with SNR set to 20 dB over a chain graph.

VII. CONCLUSIONS

This paper has studied the communication-efficient implementations of DSGD algorithms for wireless FL in fully decentralized architectures. Specifically, we have proposed generic digital and analog transmission protocols tailored to FL over wireless D2D networks by enabling broadcasting for digital transmission, and both broadcasting and AirComp for analog transmission. We also adopted a practically favourable linear compression scheme, RLC, to reduce communication burden, and implemented a consensus step size adaptive to the training iteration. For both implementations, we developed rigorous analysis framework in term of their convergence properties, characterizing the impact of the connectivity topology, the quality of transmission, and/or the channel noise on the optimality gap. Empirical experiments on an image-classification task verified the analytical results as well as the importance of an adaptive consensus step size.

APPENDIX A SCHEDULING FOR DIGITAL TRANSMISSION

At iteration t , each device $i \in \mathcal{V}$ transmits using a single time slot of the communication block in Fig. 2. The subsets of devices scheduled at each of the M slots are such that: (i) no two connected devices transmit in the same slot due to the half-duplex transmission constraints; and (ii) no two devices connected to the same device transmit in the same slot, so as not to cause interference at their common neighbor. To design a scheduling scheme with these properties, we construct an auxiliary graph $\mathcal{G}^d(\mathcal{V}, \mathcal{E}^d)$ such that the edge set $\mathcal{E}^d \supseteq \mathcal{E}$ includes not only the original edges in \mathcal{E} , but also one edge for each pair of nodes sharing one or more common neighbors. We then carry out vertex coloring on the auxiliary graph $\mathcal{G}^d(\mathcal{V}, \mathcal{E}^d)$, such that any two nodes connected by an edge are assigned with distinct “colors”. The minimum number of colors required is the *chromatic number* $\chi(\mathcal{G}^d)$ of graph $\mathcal{G}^d(\mathcal{V}, \mathcal{E}^d)$. Scheduling proceeds by assigning the nodes with the same “color” to the same slot. This ensures that both requirements (i) and (ii) above are satisfied. Transmitting nodes then broadcast to all their respective neighbors. We refer to Fig. 10 for an example.

Since finding the chromatic number $\chi(\mathcal{G}^d)$ for a general graph is an NP-hard problem, we adopt the well-known greedy algorithm, which has complexity bounded by $\mathcal{O}(|\mathcal{V}| + |\mathcal{E}^d|)$. The number M of time slots is henceforth set, for digital transmissions, to equal the number of colors obtained by the greedy algorithm. We recall that the number of colors returned by the greedy

Algorithm 2: Digital Wireless Implementation

Input : Consensus step size $\zeta^{(t)}$, SGD learning step size $\eta^{(t)}$, connectivity graph $\mathcal{G}(\mathcal{V}, \mathcal{E})$ and mixing matrix \mathbf{W}

1 Initialize at each node $i \in \mathcal{V}$: $\boldsymbol{\theta}_i^{(0)}, \hat{\boldsymbol{\theta}}_j^{(0)} = \mathbf{0}$, $\forall j \in \mathcal{N}_i \cup \{i\}$;

2 **for** $t = 0, 1, \dots, T-1$ **do**

3 **for** each device $i \in \mathcal{V}$ **do** in parallel

4 update $\boldsymbol{\theta}_i^{(t+1/2)} = \boldsymbol{\theta}_i^{(t)} - \eta^{(t)} \hat{\nabla} f_i(\boldsymbol{\theta}_i^{(t)})$;

5 **end**

6 **for** slot $s = 1, \dots, M$ **do**

7 **for** each scheduled device i at slot s **do** in parallel

8 broadcast $\mathcal{Q}_b \left(\mathbf{A}_i^{(t)} (\boldsymbol{\theta}_i^{(t+1/2)} - \hat{\boldsymbol{\theta}}_i^{(t)}) \right)$;

9 **end**

10 **for** each neighboring device $j \in \mathcal{N}_i$ **do** in parallel

11 receive $\mathcal{Q}_b \left(\mathbf{A}_j^{(t)} (\boldsymbol{\theta}_j^{(t+1/2)} - \hat{\boldsymbol{\theta}}_j^{(t)}) \right)$;

12 **end**

13 **end**

14 **for** each device $i \in \mathcal{V}$ **do** in parallel

15 update (11) and (3).

16 **end**

17 **end**

Output: $\boldsymbol{\theta}_i^{(T-1)}, \forall i \in \mathcal{V}$

algorithm is always smaller than $\Delta(\mathcal{G}^d(\mathcal{V}, \mathcal{E}^d)) + 1$, where $\Delta(\cdot)$ denotes the maximum degree of a graph [36, algorithm G].

APPENDIX B

SCHEDULING FOR ANALOG TRANSMISSION

In order to leverage AirComp in a general D2D topology, we propose a sequential scheduling policy that aims at selecting as many non-interfering star-based sub-networks as possible in each pair of time slots.

Algorithm 3: Analog Wireless Implementation

Input : Consensus step size $\zeta^{(t)}$, SGD learning step size $\eta^{(t)}$, connectivity graph $\mathcal{G}(\mathcal{V}, \mathcal{E})$, mixing matrix \mathbf{W} , transmission slots $M = 2n$, and subsets $\{\mathcal{S}_i^{\text{BT}}, \mathcal{S}_i^{\text{BR}}, \mathcal{S}_i^{\text{AT}}, \mathcal{S}_i^{\text{AR}}\}, i \in \mathcal{V}$

1 Initialize at each node $i \in \mathcal{V}$: $\boldsymbol{\theta}_i^{(0)}, \hat{\boldsymbol{\theta}}_j^{(0)} = \mathbf{0}, \forall j \in \mathcal{N}_i \cup \{i\}$, and $\hat{\mathbf{y}}_i^{(0)} = \mathbf{0}$;

2 **for** $t = 0, 1, \dots, T-1$ **do**

3 perform Line 3 - 5 in Algorithm 2;

4 **for** slot $s = 1, 3, \dots, 2n-1$ **do** *AirComp transmission*

5 **for** each node i in $\{i \in \mathcal{V} \mid s \in \mathcal{S}_i^{\text{AT}}\}$ **do** in parallel

6 | transmit to a center node j (12);

7 | **end**

8 **for** each center node j in $\{j \in \mathcal{V} \mid s \in \mathcal{S}_j^{\text{AR}}\}$ **do** in parallel

9 | receive (13) and estimate (14);

10 | **end**

11 | **end**

12 **for** slot $s = 2, 4, \dots, 2n$ **do** *BC transmission*

13 **for** each node i in $\{i \in \mathcal{V} \mid s \in \mathcal{S}_i^{\text{BT}}\}$ **do** in parallel

14 | broadcast (15);

15 | **end**

16 **for** each node j in $\{j \in \mathcal{V} \mid s \in \mathcal{S}_j^{\text{BR}}\}$ **do** in parallel

17 | receive (16) and estimate (17);

18 | **end**

19 | **end**

20 **for** each device $j \in \mathcal{V}$ **do** in parallel

21 | update (18), (22) and (23).

22 | **end**

23 **end**

Output: $\boldsymbol{\theta}_i^{(T-1)}, \forall i \in \mathcal{V}$

To this end, we first carry out the greedy coloring algorithm described in Appendix A on the original connectivity graph $\mathcal{G}^{(1)} = \mathcal{G}(\mathcal{V}, \mathcal{E})$. We define $d_c^{(1)}$ as the sum of the degrees of all nodes

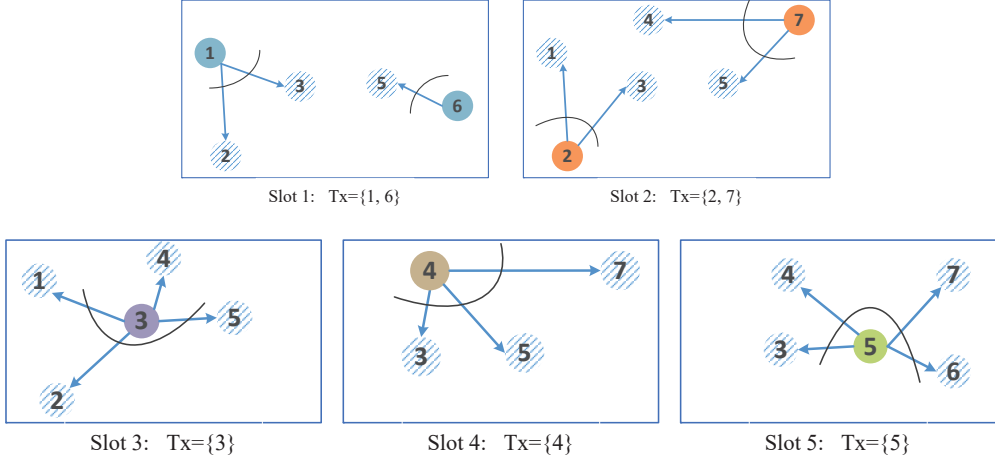


Fig. 10. An example illustrating the scheduling policy for digital transmissions in the connectivity graph of Fig. 1 ($M = 5$).

that have been assigned the same color c . Next, we set all nodes assigned the degree-maximizing color $c^* = \arg \max\{d_c^{(1)}\}$ in $\mathcal{G}^{(1)}$ as the center nodes, which compose the set $\mathcal{N}_c^{(1)}$. In the first slot of the first pair of slots, the nodes in $\mathcal{N}_c^{(1)}$ receive combined signals transmitted by their neighbors in $\mathcal{G}^{(1)}$; while, in the subsequent second slot, the same set of nodes in $\mathcal{N}_c^{(1)}$ serve broadcast transmitters. Hence, for each center node $i \in \mathcal{N}_c^{(1)}$, the first slot of the pair is in set $\mathcal{S}_i^{\text{AR}}$ and in sets $\mathcal{S}_j^{\text{AT}}$ for all nodes $j \in \mathcal{N}_i$. Conversely, the second slot is in set $\mathcal{S}_i^{\text{BT}}$ and in sets $\mathcal{S}_j^{\text{BR}}$ for all nodes $j \in \mathcal{N}_i$. The nodes in $\mathcal{N}_c^{(1)}$ and their connected edges, along with any nodes disconnected from $\mathcal{G}^{(1)}$, are then removed from $\mathcal{G}^{(1)}$ to produce the residual graph $\mathcal{G}^{(2)}$. The procedure above is repeated on this residual graph $\mathcal{G}^{(2)}$ to schedule transmissions in the next pair of slots. The overall procedure is repeated until the residual graph becomes empty, and is summarized in Algorithm 4. The number M of time slots is henceforth given by $M = 2n$.

An example can also be found in Fig. III-B. In each subfigure, only the nodes and the edges actively involved in the transmissions of the associate slot are shown. For example, although the set of neighbors of node 5 is $\mathcal{N}_5 = \{3, 4, 6, 7\}$ throughout the whole training session, node 3 is not included as an active receiver in slot 4, since it has become inactive when being “removed” from $\mathcal{G}^{(1)}$ at the end of slot 2. Furthermore, when an active transmission in the residual graph reduces to a pair of point-to-point transmission (e.g., the pair of nodes (1, 2) in slot 5), there is no difference between broadcast and Aircomp transmission. In this case, we arbitrarily assign one of the paired node (e.g., node 2) to an odd-number slot (e.g., slot 5), while assign the other node (e.g., node 1) to the subsequent even-number slot (e.g., slot 6).

Algorithm 4: Scheduling Policy for Analog Transmission

Input : $n = 0$, graph $\mathcal{G}^{(1)} = \mathcal{G}(\mathcal{V}, \mathcal{E})$

1 Initialize for each node $i \in \mathcal{N}_i$: $\mathcal{S}_i^{\text{AT}} = \mathcal{S}_i^{\text{AR}} = \mathcal{S}_i^{\text{BT}} = \mathcal{S}_i^{\text{BR}} = \emptyset$;

2 **repeat**

3 update $n = n + 1$;

4 color the graph $\mathcal{G}^{(n)}$ using the greedy algorithm described in Appendix A;

5 **foreach** center node $i \in \mathcal{N}_c^{(n)}$ **do**

6 update $\mathcal{S}_i^{\text{AR}} \leftarrow \mathcal{S}_i^{\text{AR}} \cup \{2n - 1\}$;

7 update $\mathcal{S}_i^{\text{BT}} \leftarrow \mathcal{S}_i^{\text{BT}} \cup \{2n\}$;

8 **end**

9 **foreach** center node i 's neighbors $j \in \mathcal{N}_i$ in graph $\mathcal{G}^{(n)}$ **do**

10 update $\mathcal{S}_j^{\text{AT}} \leftarrow \mathcal{S}_j^{\text{AT}} \cup \{2n - 1\}$;

11 update $\mathcal{S}_j^{\text{BR}} \leftarrow \mathcal{S}_j^{\text{BR}} \cup \{2n\}$;

12 **end**

13 update $\mathcal{V} = \mathcal{V} \setminus (\mathcal{N}_c^{(n)} \cup \{ \text{disconnected node from } \mathcal{G}^{(n)} \})$;

14 update $\mathcal{E} = \mathcal{E} \setminus (\bigcup_{i \in \mathcal{N}_c^{(n)}} (\bigcup_{j \in \mathcal{N}_i} \{(i, j)\}))$;

15 update graph $\mathcal{G}^{(n+1)} = \mathcal{G}(\mathcal{V}, \mathcal{E})$.

16 **until** $\mathcal{G}^{(n)} = \emptyset$;

Output: $M = 2n$, $\{\mathcal{S}_i^{\text{AT}}, \mathcal{S}_i^{\text{AR}}, \mathcal{S}_i^{\text{BT}}, \mathcal{S}_i^{\text{BR}}\}$, $i \in \mathcal{V}$

APPENDIX C

PROOF OF LEMMA 4.1

First, as per the definition of the linear encoding matrix $\mathbf{A} = \frac{1}{\sqrt{m}} \mathbf{H} \mathbf{R}$, it follows that $\mathbf{A} \mathbf{A}^T = \frac{1}{m} \mathbf{H} \mathbf{R} \mathbf{R}^T \mathbf{H}^T = \frac{1}{m} \mathbf{H} \mathbf{H}^T = \frac{d}{m} \mathbf{I}$.¹ In addition, by denoting the l th row of the partial Hadamard

¹We will omit the superscript $(\cdot)^{(t)}$ whenever it does not cause ambiguity throughout the appendices.

matrix \mathbf{H} by $\mathbf{h}_l^T \in \mathbb{R}^{1 \times d}$, $l = 1, \dots, m$, $\mathbb{E}[\mathbf{A}^T \mathbf{A}]$ is given by

$$\begin{aligned}
\mathbb{E}[\mathbf{A}^T \mathbf{A}] &= \frac{1}{m} \mathbb{E}[\mathbf{R}[\mathbf{h}_1, \dots, \mathbf{h}_m][\mathbf{h}_1, \dots, \mathbf{h}_m]^T \mathbf{R}] \\
&= \frac{1}{m} \mathbb{E}[[\mathbf{R}\mathbf{h}_1, \dots, \mathbf{R}\mathbf{h}_m][\mathbf{R}\mathbf{h}_1, \dots, \mathbf{R}\mathbf{h}_m]^T] \\
&= \frac{1}{m} \sum_{l=1}^m \mathbb{E}[(\mathbf{R}\mathbf{h}_l)(\mathbf{R}\mathbf{h}_l)^T] \\
&= \frac{1}{m} \sum_{l=1}^m \mathbb{E} \begin{bmatrix} r_1^2 h_{l,1}^2 & \dots & r_1 r_d h_{l,1} h_{l,d} \\ \vdots & \ddots & \vdots \\ r_1 r_d h_{l,1} h_{l,d} & \dots & r_d^2 h_{l,d}^2 \end{bmatrix} \stackrel{(a)}{=} \mathbf{I},
\end{aligned} \tag{38}$$

where $h_{l,n}$ denotes the n th entry of \mathbf{h}_l , $n = 1, \dots, d$; and (a) is due to the fact that $r_n^2 h_{l,n}^2 = 1$ for all $l = 1, \dots, m$, as well as $\mathbb{E}[r_{n_1} r_{n_2}] = 0$ for all $n_1 \neq n_2$. Then given the number of rows of \mathbf{A} , i.e., m , fixed, for all $\mathbf{u} \in \mathbb{R}^{d \times 1}$, it follows that

$$\begin{aligned}
\mathbb{E} \left\| \mathbf{u} - \frac{m}{d} \mathbf{A}^T \mathbf{A} \mathbf{u} \right\|^2 &= \mathbb{E} \left[\mathbf{u}^T \mathbf{u} - \frac{2m}{d} \mathbf{u}^T \mathbf{A}^T \mathbf{A} \mathbf{u} + \left(\frac{m}{d} \right)^2 \mathbf{u}^T \mathbf{A}^T \mathbf{A} \mathbf{A}^T \mathbf{A} \mathbf{u} \right] \\
&\stackrel{(a)}{=} \|\mathbf{u}\|^2 - \frac{m}{d} \mathbf{u}^T \mathbb{E}[\mathbf{A}^T \mathbf{A}] \mathbf{u} \stackrel{(b)}{=} \left(1 - \frac{m}{d} \right) \|\mathbf{u}\|^2,
\end{aligned} \tag{39}$$

where (a) and (b) come from $\mathbf{A} \mathbf{A}^T = \frac{d}{m} \mathbf{I}$ and (38), respectively. According to the law of iterated expectation, when $m_i^{(t)}$, $i \in \mathcal{V}$, also varies with channel state at the t th iteration, we have, for $\mathbf{A} = \frac{1}{m_i} \mathbf{H} \mathbf{R} \in \mathbb{R}^{m_i \times d}$

$$\begin{aligned}
\mathbb{E} \left\| \mathbf{u} - \frac{m_i}{d} (\mathbf{A})^T \mathcal{Q}_b(\mathbf{A} \mathbf{u}) \right\|^2 &= \mathbb{E}_{m_i} \left[\mathbb{E}_{\mathbf{A}|m_i=n} \left\| \mathbf{u} - \frac{m_i}{d} \mathbf{A}^T \mathcal{Q}_b(\mathbf{A} \mathbf{u}) \right\|^2 \right] \\
&= \sum_{n=1}^d \Pr(m_i = n) \underbrace{\mathbb{E}_{\mathbf{A}|m_i=n} \left\| \mathbf{u} - \frac{m_i}{d} \mathbf{A}^T \mathcal{Q}_b(\mathbf{A} \mathbf{u}) \right\|^2}_{\text{part I}}.
\end{aligned} \tag{40}$$

For part I, since

$$\begin{aligned}
&\mathbb{E}_{\mathbf{A}|m_i=n} \left\| \mathbf{u} - \frac{m_i}{d} \mathbf{A}^T \mathcal{Q}_b(\mathbf{A} \mathbf{u}) \right\|^2 \\
&= \mathbb{E} \left\| \left(\mathbf{u} - \frac{n}{d} \mathbf{A}^T \mathbf{A} \mathbf{u} \right) + \left(\frac{n}{d} \mathbf{A}^T \mathbf{A} \mathbf{u} - \frac{n}{d} \mathbf{A}^T \mathcal{Q}_b(\mathbf{A} \mathbf{u}) \right) \right\|^2 \\
&\stackrel{(a)}{=} \mathbb{E} \left[\left\| \mathbf{u} - \frac{n}{d} \mathbf{A}^T \mathbf{A} \mathbf{u} \right\|^2 + \frac{2n}{d} \left(\mathbf{u} - \frac{n}{d} \mathbf{A}^T \mathbf{A} \mathbf{u} \right)^T \mathbf{A}^T \mathbf{U} \mathbf{A} \mathbf{u} + \frac{n^2}{d^2} \left\| \mathbf{A}^T \mathbf{U} \mathbf{A} \mathbf{u} \right\|^2 \right] \\
&\stackrel{(b)}{=} \mathbb{E} \left\| \mathbf{u} - \frac{n}{d} \mathbf{A}^T \mathbf{A} \mathbf{u} \right\|^2 + \frac{n^2}{d^2} \mathbb{E} \left\| \mathbf{A}^T \mathbf{U} \mathbf{A} \mathbf{u} \right\|^2 \\
&\stackrel{(c)}{=} \left(1 - \frac{n}{d} + \frac{n}{d} \epsilon_b^2 \right) \|\mathbf{u}\|^2,
\end{aligned} \tag{41}$$

where $\mathbf{A}\mathbf{u} - \mathcal{Q}_b(\mathbf{A}\mathbf{u}) = \mathbf{U}\mathbf{A}\mathbf{u}$ is adopted for (a) as per IEEE 754 standard, in which $\mathbf{U} \in \mathbb{R}^{n \times n}$ is a diagonal matrix with its i th entry $[\mathbf{U}]_{ii} \triangleq u_i$, $i = 1, \dots, n$; (b) is due to the fact $\mathbf{A}\mathbf{A}^T = \frac{d}{n}\mathbf{I}$; and (c) follows from (39) as well as $\mathbb{E}[\mathbf{A}^T \mathbf{U}^2 \mathbf{A}] = \frac{1}{n} \sum_{i=1}^n |u_i|^2 \mathbf{I}$ and $|u_i| < \epsilon_b$. In addition, considering negligibly little value of ϵ_b ($\epsilon_b = 2^{-24}$ for $b = 32$ and $\epsilon_b = 2^{-53}$ for $b = 52$) [37, ch. 2], we thus safely approximate $\mathbb{E}_{\mathbf{A} \mid m_i=n} \|\mathbf{u} - \frac{m_i}{d} \mathbf{A}^T \mathcal{Q}_b(\mathbf{A}\mathbf{u})\|^2$ by $(1 - \frac{n}{d})\|\mathbf{u}\|^2$.

Next, there remains $\Pr(m_i = n)$ to calculate, $i \in \mathcal{V}$. We assume that there is at least one row for matrix $\mathbf{A}_i^{(t)}$ however adverse the channel condition is, i.e., $\Pr(m_i = 1) = \Pr(B_i/b < 2)$, and that there are no more than d rows for $\mathbf{A}_i^{(t)}$ even if the channel condition can support more than d rows, i.e. $\Pr(m_i = d) = \Pr(B_i/b \geq d)$. Furthermore, for $n = 2, \dots, d-1$, it is easy to show that

$$\begin{aligned} \Pr(m_i = n) &= \Pr(n \leq B_i/b < n+1) \\ &= \Pr\left(\min_{j \in \mathcal{N}_i} |h'_{ij}|^2 < \frac{N_0}{PM} \left(2^{(n+1)b\frac{M}{N}} - 1\right)\right) - \Pr\left(\min_{j \in \mathcal{N}_i} |h'_{ij}|^2 < \frac{N_0}{PM} \left(2^{nb\frac{M}{N}} - 1\right)\right) \\ &\stackrel{(a)}{=} G_i(n) - G_i(n+1), \end{aligned} \quad (42)$$

where the definition of function $G_i(\cdot)$ is given by (25), and (a) follows from the fact that $|h'_{ij}|^2$, $j \in \mathcal{N}_i$, are exponentially and independently distributed with mean value $A_0(\frac{d_0}{d_{ij}})^r$ such that $\Pr(\min_{j \in \mathcal{N}_i} |h'_{ij}|^2 < x) = 1 - \exp(-\frac{x}{A_0} \sum_{j \in \mathcal{N}_i} (\frac{d_{ij}}{d_0})^r)$. As a result, we have

$$\Pr(m_i = n) = \begin{cases} 1 - G_i(2), & n = 1, \\ G_i(n) - G_i(n+1), & n = 2, \dots, d-1, \\ G_i(d), & n = d. \end{cases} \quad (43)$$

Finally, Plugging (41) and (43) into (40), we arrive at (24) by constructing telescoping sums.

APPENDIX D

PROOF OF LEMMA 5.1

We substitute (13) and (16) into (14) and (17), respectively, and rewrite (18) as

$$\begin{aligned} \hat{\mathbf{y}}_j^{(t+1)} &= \hat{\mathbf{y}}_j^{(t)} + \frac{m}{d} (\mathbf{A}^{(t)})^T \mathbf{A}^{(t)} \left(\sum_{s \in \mathcal{S}_j^{\text{AR}}} \sum_{i \in \mathcal{N}_j^{(s)}} w_{ji} (\boldsymbol{\theta}_i^{(t+1/2)} - \hat{\boldsymbol{\theta}}_i^{(t)}) + \sum_{s \in \mathcal{S}_j^{\text{BR}}} w_{ji_s} (\boldsymbol{\theta}_{i_s}^{(t+1/2)} - \hat{\boldsymbol{\theta}}_{i_s}^{(t)}) \right) \\ &\quad + \frac{m}{d} (\mathbf{A}^{(t)})^T \tilde{\mathbf{n}}_j^{(t)}, \end{aligned} \quad (44)$$

in which $\tilde{\mathbf{n}}_j^{(t)}$ is the effective noise defined as

$$\tilde{\mathbf{n}}_j^{(t)} = \sum_{s \in \mathcal{S}_j^{\text{AR}}} \frac{\Re\{\mathbf{n}_j^{(t,s)}\}}{\sqrt{\gamma_j^{(t,s)}}} + \sum_{s \in \mathcal{S}_j^{\text{BR}}} \frac{w_{j,s}}{\sqrt{\alpha_{i_s}^{(t,s)}}} \Re\left\{\frac{\mathbf{n}_j^{(t,s)}}{h_{i_s,j}^{(t)}}\right\}, \quad (45)$$

which is also Gaussian with zero mean and the covariance matrix calculated as

$$\begin{aligned} \mathbb{E}[\tilde{\mathbf{n}}_j^{(t)}(\tilde{\mathbf{n}}_j^{(t)})^T] &= \sum_{s \in \mathcal{S}_j^{\text{AR}}} \frac{1}{\gamma_j^{(t,s)}} \mathbb{E}[\Re\{\mathbf{n}_j^{(t,s)}\}(\Re\{\mathbf{n}_j^{(t,s)}\})^T] + \sum_{s \in \mathcal{S}_j^{\text{BR}}} \frac{w_{j,s}^2}{\alpha_{i_s}^{(t,s)}} \mathbb{E}\left[\Re\left\{\frac{\mathbf{n}_j^{(t,s)}}{h_{i_s,j}^{(t)}}\right\}\left(\Re\left\{\frac{\mathbf{n}_j^{(t,s)}}{h_{i_s,j}^{(t)}}\right\}\right)^T\right] \\ &\stackrel{(a)}{=} \frac{N_0}{2} \left(\sum_{s \in \mathcal{S}_j^{\text{AR}}} \frac{1}{\gamma_j^{(t,s)}} + \sum_{s \in \mathcal{S}_j^{\text{BR}}} \frac{w_{j,s}^2}{\alpha_{i_s}^{(t,s)} |h_{i_s,j}^{(t)}|^2} \right) \mathbf{I}, \end{aligned} \quad (46)$$

where (a) is due to the facts that the entries $\mathbf{n}_j^{(t,s)}$ are *i.i.d.* with each denoted by $n_{j,i}^{(t,s)} \sim \mathcal{CN}(0, N_0)$, and the real and the image part of $n_{j,i}^{(t,s)}$ are also independent Gaussian random variables with zero mean and variance $\frac{N_0}{2}$, thus leading to $\sum_{s \in \mathcal{S}_j^{\text{BR}}} \frac{w_{j,s}^2}{\alpha_{i_s}^{(t,s)} |h_{i_s,j}^{(t)}|^2} \mathbb{E}[\Re\left\{\frac{\mathbf{n}_j^{(t,s)}}{h_{i_s,j}^{(t)}}\right\}(\Re\left\{\frac{\mathbf{n}_j^{(t,s)}}{h_{i_s,j}^{(t)}}\right\})^T] = \frac{N_0}{2|h_{i_s,j}^{(t)}|^2} \mathbf{I}$. Then specifying $\alpha_{i_s}^{(t,s)}$ and $\gamma_j^{(t,s)}$ by (21) and (20), respectively, we obtain (29).

Furthermore, the scheduling scheme in 4 suggests that each node is scheduled to receive as a center node for *at most one* slot (cf. Line 13 in Algorithm 4), i.e., $|\mathcal{S}_j^{\text{AR}}| \leq 1$, while it may be scheduled to receive from a broadcast Tx for *multiple* slots. In all cases, the estimate update (44) always aggregates model parameters from all of node j 's neighbors. Hence, (44) can be simplified as

$$\hat{\mathbf{y}}_j^{(t+1)} = \hat{\mathbf{y}}_j^{(t)} + \frac{m}{d} (\mathbf{A}^{(t)})^T \mathbf{A}^{(t)} \sum_{i \in \mathcal{N}_j} w_{j,i} \mathbf{u}_i^{(t)} + \frac{m}{d} (\mathbf{A}^{(t)})^T \tilde{\mathbf{n}}_j^{(t)}, \quad (47)$$

where $\theta_i^{(t+1/2)} - \hat{\theta}_i^{(t)} \triangleq \mathbf{u}_i^{(t)}$. By recursively applying (47), it follows, for any device $i \in \mathcal{V}$, that

$$\hat{\mathbf{y}}_i^{(t+1)} = \hat{\mathbf{y}}_i^{(0)} + \sum_{\tau=0}^t \left(\frac{m}{d} (\mathbf{A}^{(\tau)})^T \mathbf{A}^{(\tau)} \sum_{j \in \mathcal{N}_i} w_{i,j} \mathbf{u}_j^{(\tau)} \right) + \sum_{\tau=0}^t \frac{m}{d} (\mathbf{A}^{(\tau)})^T \tilde{\mathbf{n}}_i^{(\tau)}. \quad (48)$$

On the other hand, applying weighted sum over $j \in \mathcal{N}_i$ on both sides of (22), it follows that

$$\sum_{j \in \mathcal{N}_i} w_{i,j} \hat{\theta}_j^{(t+1)} = \sum_{j \in \mathcal{N}_i} w_{i,j} \hat{\theta}_j^{(t)} + \frac{m}{d} (\mathbf{A}^{(t)})^T \mathbf{A}^{(t)} \sum_{j \in \mathcal{N}_i} w_{i,j} \mathbf{u}_j^{(t)}. \quad (49)$$

Recursively applying (49) leads to

$$\sum_{j \in \mathcal{N}_i} w_{i,j} \hat{\theta}_j^{(t+1)} = \sum_{j \in \mathcal{N}_i} w_{i,j} \hat{\theta}_i^{(0)} + \sum_{\tau=0}^t \left(\frac{m}{d} (\mathbf{A}^{(\tau)})^T \mathbf{A}^{(\tau)} \sum_{j \in \mathcal{N}_i} w_{i,j} \mathbf{u}_j^{(\tau)} \right). \quad (50)$$

Then, combining (48) and (50) with the fact $\hat{\mathbf{y}}_i^{(0)} = \sum_{j \in \mathcal{N}_i} w_{ij} \hat{\boldsymbol{\theta}}_i^{(0)} = \mathbf{0}$, we have

$$\hat{\mathbf{y}}_i^{(t+1)} = \sum_{j \in \mathcal{N}_i} w_{ij} \hat{\boldsymbol{\theta}}_j^{(t+1)} + \sum_{\tau=0}^t \frac{m}{d} (\mathbf{A}^{(\tau)})^T \tilde{\mathbf{n}}_i^{(\tau)}. \quad (51)$$

By substituting (51) for $\hat{\mathbf{y}}_i^{(t+1)}$ in device i 's consensus update for analog implementation, (23) can be recast as (28).

APPENDIX E PROOF OF LEMMA 5.2

To prove Lemma 5.2, we first provide variants of [21, Lemma 17 and Lemma 18], where matrix notations are used for the simplicity of notation.

Lemma E.1 (Variant of [21, Lemma 17]): Denoting $[\boldsymbol{\theta}_1^{(t)}, \dots, \boldsymbol{\theta}_K^{(t)}] \in \mathbb{R}^{d \times K}$, $[\hat{\boldsymbol{\theta}}_1^{(t)}, \dots, \hat{\boldsymbol{\theta}}_K^{(t)}] \in \mathbb{R}^{d \times K}$, $[\bar{\boldsymbol{\theta}}^{(t)}, \dots, \bar{\boldsymbol{\theta}}^{(t)}] \in \mathbb{R}^{d \times K}$ and $[\tilde{\mathbf{n}}_1^{(t)}, \dots, \tilde{\mathbf{n}}_K^{(t)}] \in \mathbb{R}^{d \times K}$, by $\boldsymbol{\Theta}^{(t)}$, $\hat{\boldsymbol{\Theta}}^{(t)}$, $\bar{\boldsymbol{\Theta}}^{(t)}$ and $\tilde{\mathbf{N}}^{(t)}$, respectively, then for consensus step size $\zeta^{(t)} \geq 0$, mixing matrix \mathbf{W} and any parameter $\alpha_1 > 0$, on average over RLC and AWGN, we have

$$\begin{aligned} \mathbb{E} \|\boldsymbol{\Theta}^{(t+1)} - \bar{\boldsymbol{\Theta}}^{(t+1)}\|_F^2 &\leq (1 + \alpha_1) (1 - \delta \zeta^{(t)})^2 \mathbb{E} \|\boldsymbol{\Theta}^{(t+1/2)} - \bar{\boldsymbol{\Theta}}^{(t+1/2)}\|_F^2 + \\ &\quad (1 + \alpha_1^{-1}) \beta^2 (\zeta^{(t)})^2 \mathbb{E} \|\boldsymbol{\Theta}^{(t+1/2)} - \hat{\boldsymbol{\Theta}}^{(t+1)}\|_F^2 + (\zeta^{(t)})^2 \omega^2 d \sum_{\tau=0}^t \tilde{N}_0^{(\tau)}, \end{aligned} \quad (52)$$

where $\tilde{N}_0^{(\tau)} = \sum_{i \in \mathcal{V}} \tilde{N}_{0i}^{(\tau)}$ is the sum-variance of effective noise over all devices.

Proof: With the fact $(\mathbf{W} - \mathbf{I})\mathbf{1}\mathbf{1}^T/K = \mathbf{0}$, rewrite (28) and (30) in matrix forms as $\boldsymbol{\Theta}^{(t+1)} = \boldsymbol{\Theta}^{(t+1/2)} + \zeta^{(t)} \hat{\boldsymbol{\Theta}}^{(t+1)} (\mathbf{W} - \mathbf{I}) + \zeta^{(t)} \omega \sum_{\tau=0}^t (\mathbf{A}^{(\tau)})^T \tilde{\mathbf{N}}^{(\tau)}$ and $\bar{\boldsymbol{\Theta}}^{(t+1)} = \bar{\boldsymbol{\Theta}}^{(t+1/2)} + \zeta^{(t)} \omega \sum_{\tau=0}^t (\mathbf{A}^{(\tau)})^T \tilde{\mathbf{N}}^{(\tau)} \mathbf{1}\mathbf{1}^T/K$, respectively. Then, we have

$$\begin{aligned} &\mathbb{E} \|\boldsymbol{\Theta}^{(t+1)} - \bar{\boldsymbol{\Theta}}^{(t+1)}\|_F^2 \\ &= \mathbb{E} \left\| \boldsymbol{\Theta}^{(t+1/2)} - \bar{\boldsymbol{\Theta}}^{(t+1/2)} + \zeta^{(t)} \hat{\boldsymbol{\Theta}}^{(t+1)} (\mathbf{W} - \mathbf{I}) + \zeta^{(t)} \omega \sum_{\tau=0}^t (\mathbf{A}^{(\tau)})^T \tilde{\mathbf{N}}^{(\tau)} \left(\mathbf{I} - \frac{\mathbf{1}\mathbf{1}^T}{K} \right) \right\|_F^2 \\ &\stackrel{(a)}{=} \mathbb{E} \left\| \boldsymbol{\Theta}^{(t+1/2)} - \bar{\boldsymbol{\Theta}}^{(t+1/2)} + \zeta^{(t)} \hat{\boldsymbol{\Theta}}^{(t+1)} (\mathbf{W} - \mathbf{I}) \right\|_F^2 + (\zeta^{(t)})^2 \omega^2 \mathbb{E} \left\| \sum_{\tau=0}^t (\mathbf{A}^{(\tau)})^T \tilde{\mathbf{N}}^{(\tau)} \left(\mathbf{I} - \frac{\mathbf{1}\mathbf{1}^T}{K} \right) \right\|_F^2 \\ &\stackrel{(b)}{\leq} \mathbb{E} \left\| (\boldsymbol{\Theta}^{(t+1/2)} - \bar{\boldsymbol{\Theta}}^{(t+1/2)}) (\mathbf{I} + \zeta^{(t)} (\mathbf{W} - \mathbf{I})) + \zeta^{(t)} (\hat{\boldsymbol{\Theta}}^{(t+1)} - \boldsymbol{\Theta}^{(t+1/2)}) (\mathbf{W} - \mathbf{I}) \right\|_F^2 \\ &\quad + (\zeta^{(t)})^2 \omega^2 d \left(1 - \frac{1}{K} \right) \sum_{\tau=0}^t \tilde{N}_0^{(\tau)} \stackrel{(c)}{\leq} \text{RHS of (52)}, \end{aligned}$$

where (a) is due to the expectation taken over Gaussian noise and RLC, i.e., $\mathbb{E}[(\mathbf{A}^{(\tau)})^T \tilde{\mathbf{N}}^{(\tau)}]$, is zero; the first term in (b) is as a result of $\bar{\mathbf{X}}(\mathbf{W} - \mathbf{I}) = \mathbf{0}$ for any $\mathbf{X} \in \mathbb{R}^{d \times K}$; the second term in (b) is based on $\mathbf{A}^{(\tau)}(\mathbf{A}^{(\tau)})^T = \frac{d}{m}\mathbf{I}$ and *i.i.d.* entries of $\tilde{\mathbf{n}}_i^{(\tau)}$ such that $\mathbb{E}\|\tilde{\mathbf{n}}_i^{(\tau)}\|^2 = m\tilde{N}_{0i}^{(\tau)}$ with $\sum_{i \in \mathcal{V}} \tilde{N}_{0i}^{(\tau)} \triangleq \tilde{N}_0^{(\tau)}$; and (c) follows [21, Lemma 17]. \blacksquare

Lemma E.2 (Variant of [21, Lemma 18]): In addition to $\Theta^{(t)}$, $\hat{\Theta}^{(t)}$, $\bar{\Theta}^{(t)}$ and $\tilde{\mathbf{N}}^{(t)}$ denoted as in Lemma E.1, denoting $[\hat{\nabla}f_1(\boldsymbol{\theta}_1^{(t)}), \dots, \hat{\nabla}f_K(\boldsymbol{\theta}_K^{(t)})] \in \mathbb{R}^{d \times K}$ by $\hat{\nabla}F^{(t)}$, then for consensus step size $\zeta^{(t)} \geq 0$, mixing matrix \mathbf{W} and any parameter $\alpha_2 > 0$, on average over RLC and AWGN, we have

$$\begin{aligned} \mathbb{E}\|\Theta^{(t+3/2)} - \hat{\Theta}^{(t+2)}\|_F^2 &\leq (1 + \alpha_2^{-1})(1 - \omega)\beta^2(\zeta^{(t)})^2 \mathbb{E}\|\Theta^{(t+1/2)} - \eta^{(t+1)}\hat{\nabla}F^{(t+1)} - \bar{\Theta}^{(t+1/2)}\|_F^2 + \\ &\quad (1 + \alpha_2)(1 - \omega)(1 + \beta\zeta^{(t)})^2 \mathbb{E}\|\Theta^{(t+1/2)} - \eta^{(t+1)}\hat{\nabla}F^{(t+1)} - \hat{\Theta}^{(t+1)}\|_F^2 + \\ &\quad (\zeta^{(t)})^2(1 - \omega)\omega^2 d \sum_{\tau=0}^t \tilde{N}_0^{(\tau)}. \end{aligned} \quad (53)$$

Proof: Given the constant $\omega = m/d$ in analog implementation, (22) implies that, for $i \in \mathcal{V}$,

$$\hat{\Theta}_i^{(t+1)} = \hat{\Theta}_i^{(t)} + \omega(\mathbf{A}^{(t)})^T \mathbf{A}^{(t)}(\Theta_i^{(t+1/2)} - \hat{\Theta}_i^{(t)}). \quad (54)$$

Therefore, substituting (54) for $\hat{\Theta}^{(t+2)}$, it follows that

$$\begin{aligned} \mathbb{E}\|\Theta^{(t+3/2)} - \hat{\Theta}^{(t+2)}\|_F^2 &= \mathbb{E}\left\|\Theta^{(t+3/2)} - \left(\hat{\Theta}_i^{(t+1)} + \omega(\mathbf{A}^{(t+1)})^T \mathbf{A}^{(t+1)}(\Theta_i^{(t+3/2)} - \hat{\Theta}_i^{(t+1)})\right)\right\|_F^2 \\ &= \mathbb{E}\left\|(\Theta^{(t+3/2)} - \hat{\Theta}_i^{(t+1)}) - \omega(\mathbf{A}^{(t+1)})^T \mathbf{A}^{(t+1)}(\Theta_i^{(t+3/2)} - \hat{\Theta}_i^{(t+1)})\right\|_F^2 \\ &\stackrel{(a)}{=} (1 - \omega)\mathbb{E}\|\Theta^{(t+3/2)} - \hat{\Theta}^{(t+1)}\|_F^2 \stackrel{(b)}{=} (1 - \omega)\mathbb{E}\|\Theta^{(t+1)} - \eta^{(t+1)}\hat{\nabla}F^{(t+1)} - \hat{\Theta}^{(t+1)}\|_F^2 \stackrel{(c)}{=} (1 - \omega) \\ &\quad \mathbb{E}\left\|\Theta^{(t+1/2)} - \eta^{(t+1)}\hat{\nabla}F^{(t+1)} + \zeta^{(t)}\hat{\Theta}^{(t+1)}(\mathbf{W} - \mathbf{I}) - \hat{\Theta}^{(t+1)} + \zeta^{(t)}\omega \sum_{\tau=0}^t (\mathbf{A}^{(\tau)})^T \tilde{\mathbf{N}}^{(\tau)}\right\|_F^2 \\ &\stackrel{(d)}{\leq} (1 - \omega)\left(\mathbb{E}\|\Theta^{(t+1/2)} - \eta^{(t+1)}\hat{\nabla}F^{(t+1)} + \zeta^{(t)}\hat{\Theta}^{(t+1)}(\mathbf{W} - \mathbf{I}) - \hat{\Theta}^{(t+1)}\|_F^2 + \right. \\ &\quad \left.\mathbb{E}\left\|\zeta^{(t)}\omega \sum_{\tau=0}^t (\mathbf{A}^{(\tau)})^T \tilde{\mathbf{N}}^{(\tau)}\right\|_F^2\right) \\ &\stackrel{(e)}{\leq} (1 - \omega)\left((1 + \alpha_2^{-1})\beta^2(\zeta^{(t)})^2 \mathbb{E}\|\Theta^{(t+1/2)} - \eta^{(t+1)}\hat{\nabla}F^{(t+1)} - \bar{\Theta}^{(t+1/2)}\|_F^2 + \right. \\ &\quad \left.(1 + \alpha_2)(1 + \beta\zeta^{(t)})^2 \mathbb{E}\|\Theta^{(t+1/2)} - \eta^{(t+1)}\hat{\nabla}F^{(t+1)} - \hat{\Theta}^{(t+1)}\|_F^2 + (\zeta^{(t)})^2\omega^2 d \sum_{\tau=0}^t \tilde{N}_0^{(\tau)}\right), \end{aligned}$$

where (a) is based on (39); (b) executes one SGD step (cf. (1)); (c) is due to the analog consensus update (cf. (28)); (d) is as a results of zero-mean AWGN; and (e) follows [21, Lemma 18] combining with the noise variance as derived similarly in the proof for Lemma E.2. ■

We elaborate on non-trivial modifications made based on [21, Appendix C] in the sequel.² First, we need to modify two auxiliary functions to be adaptive as below:

$$\eta_1(\zeta^{(t)}) = (1 + \alpha_1)(1 - \delta\zeta^{(t)})^2 + (1 + \alpha_2^{-1})(1 - \omega)\beta^2(\zeta^{(t)})^2, \quad (55)$$

$$\xi_1(\zeta^{(t)}) = (1 + \alpha_1^{-1})\beta^2(\zeta^{(t)})^2 + (1 + \alpha_2)(1 - \omega)(1 + \beta\zeta^{(t)})^2, \quad (56)$$

and introduce another auxiliary function defined as

$$\eta_2(x) = \left(\frac{\delta^2}{4} + \frac{2}{\omega}\beta^2 \right) x^2 - \delta x + 1 = 1 - \tilde{p}(x), \quad (57)$$

where

$$\tilde{p}(x) = \delta x - \left(\frac{\delta^2}{4} + \frac{2}{\omega}\beta^2 \right) x^2. \quad (58)$$

According to the definition of function $\eta_2(x)$, which is a quadratic convex function decreasing over $[0, x^*]$ with $x^* = \min_x \eta_2(x)$, it follows that $\tilde{p}(x)$ increases over $[0, x^*]$.

Next, we substitute $\zeta^{(t)} = \frac{\zeta_0}{\sqrt[4]{\tilde{N}_0 t / a' + 1}}$ for x in $\tilde{p}(x)$ to obtain function $\tilde{p}^{(t)} : \mathbb{R}_+ \mapsto \mathbb{R}$ in (33). Note that since ζ_0 given in Theorem 4.1 is given by $\zeta_0 = \lambda' x^*$ for a specific choice $\lambda' = \frac{8\beta^2 + \delta^2\omega}{2(16\delta + \delta^2 + 4\beta^2 + 2\delta\beta^2 - 8\delta\omega)} \in (0, 1]$ (see [21, (20), (24)] for detail), it follows that $\zeta^{(t)} \leq \zeta^{(0)} = \zeta_0 \leq x^*$. As we establish the facts that $\zeta^{(t)} \in [0, x^*]$ decreases over $t \geq 0$ and $\tilde{p}(x)$ increases over $[0, x^*]$, $\tilde{p}^{(t)}$ turns out to be decreasing over $t \geq 0$ according to the composition of monotonic functions. Furthermore, based on the relation of $\eta_1(x) \leq \eta_2(x)$ derived in [21, Appendix C], which holds for any x and $\omega > 0$, since

$$\eta_1(\zeta_0) \leq \eta_2(\zeta_0) = 1 - \tilde{p}(\zeta_0) \stackrel{(33)}{=} 1 - \tilde{p}^{(0)} \stackrel{[21, (24)]}{\leq} 1 - p(\delta, \omega), \quad (59)$$

it implies that $p(\delta, \omega) \leq \tilde{p}^{(0)}$.

In addition, we have

$$\eta_1(\zeta^{(t)}) \leq \eta_2(\zeta^{(t)}) = 1 - \tilde{p}(\zeta^{(t)}) \stackrel{(33)}{=} 1 - \tilde{p}^{(t)}, \quad (60)$$

²We will omit the dependence of functions on δ and ω but the iteration index t throughout the appendices, as long as it does not cause any ambiguity in the context.

and

$$\xi_1(\zeta^{(t)}) \stackrel{(a)}{\leq} \xi_1(\zeta_0) \stackrel{[21], (26)}{\leq} 1 - p(\delta, \omega), \quad (61)$$

where (a) is due to the fact that function $\xi_1(\zeta^{(t)})$ increases over $\zeta^{(t)} > 0$ and $\zeta^{(t)} \leq \zeta_0$. Finally, combining (60) and (61), we arrive at the following variant of [21, (21)]

$$\begin{aligned} \max \{ \eta_1(\zeta^{(t)}), \xi_1(\zeta^{(t)}) \} &\leq \max \{ 1 - \tilde{p}^{(t)}, 1 - p(\delta, \omega) \} \\ &= 1 - \min \{ \tilde{p}^{(t)}, p(\delta, \omega) \} \stackrel{(32)}{=} 1 - p^{(t)}. \end{aligned} \quad (62)$$

Now, we are ready to derive the recursive upper-bound given by (35). The following basic inequalities are frequently recalled in the sequel, which are, for two given matrices \mathbf{X} and \mathbf{Y} of the same size,

$$\|\mathbf{X} + \mathbf{Y}\|_F^2 \leq (1 + \alpha)\|\mathbf{X}\|_F^2 + (1 + \alpha^{-1})\|\mathbf{Y}\|_F^2, \quad \forall \alpha > 0, \quad (63)$$

and for another square matrix \mathbf{Z} ,

$$\|\mathbf{X}\mathbf{Z}\|_F \leq \|\mathbf{X}\|_F \|\mathbf{Z}\|_2. \quad (64)$$

By applying one SGD step (cf. (1)), it follows that, for any given $\alpha_3 > 0$,

$$\begin{aligned} \mathbb{E}\|\Theta^{(t+1/2)} - \bar{\Theta}^{(t+1/2)}\|_F^2 &= \mathbb{E}\left\|(\Theta^{(t)} - \bar{\Theta}^{(t)}) - \eta^{(t)}\hat{\nabla}F^{(t)}\left(\mathbf{I} - \frac{\mathbf{1}\mathbf{1}^T}{K}\right)\right\|_F^2 \\ &\stackrel{(63),(64)}{\leq} (1 + \alpha_3^{-1})\mathbb{E}\|\Theta^{(t)} - \bar{\Theta}^{(t)}\|_F^2 + (1 + \alpha_3)(\eta^{(t)})^2\mathbb{E}\|\hat{\nabla}F^{(t)}\|_F^2\left\|\mathbf{I} - \frac{\mathbf{1}\mathbf{1}^T}{K}\right\| \\ &\stackrel{(7)}{\leq} (1 + \alpha_3^{-1})\mathbb{E}\|\Theta^{(t)} - \bar{\Theta}^{(t)}\|_F^2 + (1 + \alpha_3)K(\eta^{(t)})^2G^2. \end{aligned} \quad (65)$$

Similarly, for the same choice of α_3 , it is also true that

$$\begin{aligned} &\mathbb{E}\|\Theta^{(t+1/2)} - \eta^{(t+1)}\hat{\nabla}F^{(t+1)} - \bar{\Theta}^{(t+1/2)}\|_F^2 \\ &\stackrel{(63)}{\leq} (1 + \alpha_3^{-1})\mathbb{E}\|\Theta^{(t)} - \bar{\Theta}^{(t)}\|_F^2 + (1 + \alpha_3)\mathbb{E}\left\|\eta^{(t)}\hat{\nabla}F^{(t)}\left(\mathbf{I} - \frac{\mathbf{1}\mathbf{1}^T}{K}\right) + \eta^{(t+1)}\hat{\nabla}F^{(t+1)}\right\|_F^2 \\ &\stackrel{(7)}{\leq} (1 + \alpha_3^{-1})\mathbb{E}\|\Theta^{(t)} - \bar{\Theta}^{(t)}\|_F^2 + 6(1 + \alpha_3)K(\eta^{(t)})^2G^2, \end{aligned} \quad (66)$$

and

$$\begin{aligned} \mathbb{E}\|\Theta^{(t+1/2)} - \eta^{(t+1)}\hat{\nabla}F^{(t+1)} - \hat{\Theta}^{(t+1)}\|_F^2 &\stackrel{(63),(7)}{\leq} (1 + \alpha_3^{-1})\|\Theta^{(t+1/2)} - \bar{\Theta}^{(t+1)}\|_F^2 + \\ &\quad (1 + \alpha_3)K(\eta^{(t)})^2G^2. \end{aligned} \quad (67)$$

Then, combining (52) and (53), where relevant terms are substituted by (65)-(67), after some manipulations, we have

$$\begin{aligned}
e^{(t+1)} &\stackrel{(31)}{\leq} \eta_1(\zeta^{(t)})(1 + \alpha_3^{-1})\mathbb{E}\|\Theta^{(t)} - \bar{\Theta}^{(t)}\|_F^2 + \xi_1(\zeta^{(t)})(1 + \alpha_3^{-1})\|\Theta^{(t+1/2)} - \hat{\Theta}^{(t+1)}\|_F^2 + \\
&\quad (\eta_1(\zeta^{(t)}) + \xi_1(\zeta^{(t)}))(1 + \alpha_3)(\eta^{(t)})^2 6KG^2 + (\zeta^{(t)})^2(2 - \omega)\omega^2 d \sum_{\tau=0}^t \tilde{N}_0^{(\tau)} \\
&\leq \underbrace{\max\{\eta_1(\zeta^{(t)}), \xi_1(\zeta^{(t)})\} (1 + \alpha_3^{-1})e^{(t)} + 12 \max\{\eta_1(\zeta^{(t)}), \xi_1(\zeta^{(t)})\} (1 + \alpha_3)(\eta^{(t)})^2 KG^2 +}_{\text{part I}} \\
&\quad \underbrace{(\zeta^{(t)})^2(2 - \omega)\omega^2 d \sum_{\tau=0}^t \tilde{N}_0^{(\tau)}}_{\text{part II}}. \quad (68)
\end{aligned}$$

Note that by using (62) and choosing $\alpha_1 = \frac{\delta\zeta^{(t)}}{2}$, $\alpha_2 = \frac{\omega}{2}$ and $\alpha_3 = \frac{p^{(t)}}{2}$ [21, (20), Lemma 21], part I in (68) proves to be $(1 - \frac{p^{(t)}}{2})e^{(t)} + \frac{2}{p^{(t)}}(\eta^{(t)})^2 12KG^2$. Furthermore, looking into part II, we have

$$\begin{aligned}
(\zeta^{(t)})^2 \sum_{\tau=0}^t \tilde{N}_0^{(\tau)} &\stackrel{(a)}{\leq} \frac{(\zeta^{(t)})^2}{p^{(t)}} p^{(t)} t \tilde{N}_0 \stackrel{(b)}{\leq} \frac{(\zeta^{(t)})^2}{p^{(t)}} \tilde{p}^{(t)} \left(\sqrt[4]{\tilde{N}_0 t / a'} \right) a' \tilde{N}_0^{\frac{3}{4}} \\
&\stackrel{(c)}{\leq} \frac{\delta\zeta_0}{p^{(t)}} (\zeta^{(t)})^2 \frac{1}{\sqrt[4]{\tilde{N}_0 t / a' + 1}} \left(\sqrt[4]{\tilde{N}_0 t / a'} + 1 \right) a' \tilde{N}_0^{\frac{3}{4}} \stackrel{(d)}{=} \frac{\delta\zeta_0}{p^{(t)}} \left(\frac{\zeta_0 a' / \sqrt[4]{\tilde{N}_0}}{t + a' / \sqrt[4]{\tilde{N}_0}} \right)^2 a' \tilde{N}_0^{\frac{3}{4}} \\
&= \frac{1}{p^{(t)}} \left(\frac{\mu}{3.25} \right)^2 \left(\frac{3.25/\mu}{t + a' / \sqrt[4]{\tilde{N}_0}} \right)^2 \delta(\zeta_0 a')^3 \sqrt[4]{\tilde{N}_0} \\
&\stackrel{(e)}{\leq} \frac{1}{p^{(t)}} \left(\frac{\mu}{3.25} \right)^2 (\eta^{(t)})^2 \delta(\zeta_0 a')^3 \sqrt[4]{\tilde{N}_0}, \quad (69)
\end{aligned}$$

where (a) is due to $\tilde{N}_{0,T} = \max_{t \in \{0, \dots, T-1\}} \{\tilde{N}_0^{(t)}\}$; (b) is as a result of $p^{(t)} \leq \tilde{p}^{(t)}$ (cf. (32)); (c) is because of $\tilde{p}^{(t)} \leq \frac{\delta\zeta_0}{\sqrt[4]{\tilde{N}_0 t / a' + 1}}$ (cf. (33)); (d) is by definition of $\zeta^{(t)} = \frac{\zeta_0}{\sqrt[4]{\tilde{N}_0 t / a' + 1}}$; and (e) results from $\eta^{(t)} = \frac{3.25}{\mu} \frac{1}{t+a}$ with $a < a' / \sqrt[4]{\tilde{N}_0}$.

Finally, plugging the above results for part I and part II into (68), we complete the proof for Lemma 5.2.

APPENDIX F

PROOF OF THEOREM 5.1

Since $\tilde{p}^{(t)}$ is decreasing over $t \geq 0$, by definition of $p^{(t)}(\delta, \omega)$ in (32), $p^{(t)}(\delta, \omega)$ proves to be non-increasing over $t \geq 0$. Hence, $p^{(t)}(\delta, \omega) \geq p^{(T)}(\delta, \omega)$, and we can further upper bound the

RHS of (35) by replacing $p^{(t)}(\delta, \omega)$ with $p^{(T)}(\delta, \omega)$. Based on Lemma 5.2, we have the exact upper bound for $e^{(t)}$ given by [21, Lemma 22]

$$e^{(t)} \leq \frac{10}{(p^{(T)}(\delta, \omega))^2} (\eta^{(t)})^2 \left(24KG^2 + A(\delta, \omega) \sqrt[4]{\tilde{N}_0} \right). \quad (70)$$

Then, by definition of $e^{(t)}$ (cf. (31)), we have

$$\sum_{i \in \mathcal{V}} \mathbb{E} \|\bar{\boldsymbol{\theta}}^{(t)} - \boldsymbol{\theta}_i^{(t)}\|^2 \leq \frac{10}{(p^{(T)}(\delta, \omega))^2} (\eta^{(t)})^2 \left(24KG^2 + A(\delta, \omega) \sqrt[4]{\tilde{N}_0} \right). \quad (71)$$

Next, to prove Theorem 5.1, we need to revisit [21, Lemma 20] as follows.

$$\begin{aligned} \mathbb{E} \|\bar{\boldsymbol{\theta}}^{(t+1)} - \boldsymbol{\theta}^*\|^2 &\stackrel{(1)}{=} \mathbb{E} \left\| \bar{\boldsymbol{\theta}}^{(t)} - \eta^{(t)} \frac{1}{K} \sum_{i \in \mathcal{V}} \hat{\nabla} f_i(\boldsymbol{\theta}_i^{(t)}) + \zeta^{(t)} \frac{1}{K} \sum_{i \in \mathcal{V}} \sum_{\tau=0}^t \frac{m}{d} (\mathbf{A}^{(\tau)})^T \tilde{\mathbf{n}}_i^{(\tau)} - \boldsymbol{\theta}^* \right\|^2 \\ &\stackrel{(a)}{=} \underbrace{\mathbb{E} \left\| \bar{\boldsymbol{\theta}}^{(t)} - \eta^{(t)} \frac{1}{K} \sum_{i \in \mathcal{V}} \hat{\nabla} f_i(\boldsymbol{\theta}_i^{(t)}) - \boldsymbol{\theta}^* \right\|^2}_{\text{part I}} + \underbrace{\mathbb{E} \left\| \zeta^{(t)} \frac{1}{K} \sum_{i \in \mathcal{V}} \sum_{\tau=0}^t \frac{m}{d} (\mathbf{A}^{(\tau)})^T \tilde{\mathbf{n}}_i^{(\tau)} \right\|^2}_{\text{part II}}, \end{aligned}$$

where (a) is as a result of $\mathbb{E}[(\mathbf{A}^{(\tau)})^T \tilde{\mathbf{n}}_i^{(\tau)}] = 0$. As for Part I, [21, Lemma 20] can be directly applied, while, for part II, we need to relate it to terms involving learning rate $\eta^{(t)}$ as

$$\begin{aligned} \mathbb{E} \left\| \zeta^{(t)} \frac{1}{K} \sum_{i \in \mathcal{V}} \sum_{\tau=0}^t \frac{m}{d} (\mathbf{A}^{(\tau)})^T \tilde{\mathbf{n}}_i^{(\tau)} \right\|^2 &= \frac{1}{K^2} \frac{m^2}{d^2} (\zeta^{(t)})^2 \sum_{\tau=0}^t \sum_{i \in \mathcal{V}} \mathbb{E} \|(\mathbf{A}^{(\tau)})^T \tilde{\mathbf{n}}_i^{(\tau)}\|^2 \\ &\stackrel{(a)}{=} \frac{1}{K^2} \frac{m^2}{d} (\zeta^{(t)})^2 \sum_{\tau=0}^t \tilde{N}_0^{(\tau)} \stackrel{(34)}{\leq} \frac{1}{K^2} \frac{m^2}{d} (\zeta^{(t)})^2 t \tilde{N}_{0,T} \\ &\leq \frac{1}{K^2} \frac{m^2}{d} \zeta^{(t)} \frac{\zeta_0(\delta, \omega)}{\sqrt[4]{\tilde{N}_0} t / a' + 1} \left(\sqrt[4]{\tilde{N}_0} t / a' + 1 \right) a' \tilde{N}_{0,T}^{\frac{3}{4}} \\ &= \frac{1}{K^2} \frac{m^2}{d} \frac{\mu}{3.25} \frac{3.25/\mu}{t + a' / \sqrt[4]{\tilde{N}_0}} (\zeta_0(\delta, \omega) a')^2 \sqrt{\tilde{N}_{0,T}} \\ &\stackrel{(b)}{\leq} \frac{1}{K^2} \omega^2 d \frac{\mu}{3.25} \eta^{(t)} (\zeta_0(\delta, \omega) a')^2 \sqrt{\tilde{N}_{0,T}}, \end{aligned} \quad (72)$$

where (a) follows from $\mathbf{A}^{(\tau)} (\mathbf{A}^{(\tau)})^T = \frac{d}{m} \mathbf{I}$ and $\mathbb{E} \|\tilde{\mathbf{n}}_i^{(\tau)}\|^2 = m \tilde{N}_{0i}^{(\tau)}$; and (b) is due to $a < a' / \sqrt[4]{\tilde{N}_0}$ and $\omega = m/d$, as well as definition of $\eta^{(t)} = \frac{3.25}{\mu} \frac{1}{t+a}$.

With part II replaced by the RHS of (72), we obtain the following lemma.

Lemma F.1 (Variant of [21, Lemma 20]): Denoting the optimal solution to (P0) by $\boldsymbol{\theta}^*$ and the corresponding objective value $F(\boldsymbol{\theta}^*)$ by F^* , the average of iterates $\bar{\boldsymbol{\theta}}^{(t+1)}$ satisfies

$$\begin{aligned} \mathbb{E} \|\bar{\boldsymbol{\theta}}^{(t+1)} - \boldsymbol{\theta}^*\|^2 &\leq (1 - \eta^{(t)} \mu) \mathbb{E} \|\bar{\boldsymbol{\theta}}^{(t)} - \boldsymbol{\theta}^*\|^2 + \eta^{(t)} \frac{1}{K^2} \omega^2 d \frac{\mu}{3.25} (\zeta_0(\delta, \omega) a')^2 \sqrt{\tilde{N}_{0,T}} + (\eta^{(t)})^2 \frac{\bar{\sigma}^2}{K} \\ &\quad + 2\eta^{(t)} (2\eta^{(t)} L - 1) (\mathbb{E}[F(\bar{\boldsymbol{\theta}}^{(t)})] - F^*) + \eta^{(t)} \frac{2\eta^{(t)} L^2 + L}{K} \sum_{i \in \mathcal{V}} \mathbb{E} \|\bar{\boldsymbol{\theta}}^{(t)} - \boldsymbol{\theta}_i^{(t)}\|^2. \end{aligned} \quad (73)$$

Since $\eta^{(t)} \leq \eta^{(0)} = \frac{3.25}{\mu a}$, and $a \geq \frac{13L}{\mu}$, it follows that $\eta^{(t)} \leq \frac{1}{4L}$ thus leading to $2L\eta^{(t)} - 1 \leq -0.5$ and $2\eta^{(t)}L^2 + L \leq 1.5L$. With this fact and the upper bound on the consensus error given by (71), (73) implies that

$$\begin{aligned} v_e^{(t+1)} &\leq (1 - \eta^{(t)}\mu)v_e^{(t)} - \eta^{(t)}f_e^{(t)} + \eta^{(t)}\frac{1}{K^2}\omega^2d\frac{\mu}{3.25}(\zeta_0(\delta, \omega)a')^2\sqrt{\tilde{N}_{0,T}} + \\ &\quad (\eta^{(t)})^2\frac{\bar{\sigma}^2}{K} + (\eta^{(t)})^3\frac{15L}{(p^{(T)}(\delta, \omega))^2}\left(24G^2 + \frac{A(\delta, \omega)}{K}\sqrt{\tilde{N}_{0,T}}\right), \end{aligned} \quad (74)$$

where $v_e^{(t)} = \mathbb{E}\|\bar{\theta}^{(t)} - \theta^*\|^2$ and $f_e^{(t)} = \mathbb{E}[F(\bar{\theta}^{(t)})] - F^*$ measure, on average over RLC, the distance to the optimal solution and the optimality gap to the objective value for problem (P0), respectively. Note that the standard result in [38, Lemma 3.3] is not applicable to (74) to characterize the optimality gap due to the absence of linear terms w.r.t $\eta^{(t)}$. To capture the performance of the optimality-gap sequence $\{f_e^{(t)}\}$, we need the following lemma.

Lemma F.2 (Variant of [38, Lemma 3.3]): For non-negative sequences $\{v_e^{(t)}\}$ and $\{f_e^{(t)}\}$, $\eta^{(t)} = \frac{3.25}{\mu}\frac{1}{t+a}$ with $\mu > 0$ and $a > 1$, and constants $A, B, C \geq 0$, where $t = 0, \dots, T-1$, such that

$$v_e^{(t+1)} \leq (1 - \eta^{(t)}\mu)v_e^{(t)} + \eta^{(t)}A + (\eta^{(t)})^2B + (\eta^{(t)})^3C - \eta^{(t)}f_e^{(t)}, \quad (75)$$

we have

$$\frac{1}{S_T} \sum_{t=0}^{T-1} w^{(t)}f_e^{(t)} \leq \frac{\mu}{3.25} \frac{a^3 - 3.25a^2}{S_T} v_e^{(0)} + A + \frac{1.625(2a+T)T}{\mu S_T} B + \frac{3.25^2 T}{\mu^2 S_T} C, \quad (76)$$

where $w^{(t)} = (a+t)^2$ and $S_T = \sum_{t=0}^{T-1} w^{(t)}$.

Proof: Following similar procedures as that for proving [38, Lemma 3.3], first, multiplying $\frac{w^{(t)}}{\eta^{(t)}}$ with both sides of (75), we have

$$v_e^{(t+1)} \frac{w^{(t)}}{\eta^{(t)}} \leq (1 - \eta^{(t)}\mu) \frac{w^{(t)}}{\eta^{(t)}} v_e^{(t)} + w^{(t)}A + w^{(t)}\eta^{(t)}B + w^{(t)}(\eta^{(t)})^2C - w^{(t)}f_e^{(t)}. \quad (77)$$

To obtain the same relation $(1 - \eta^{(t)}\mu) \frac{w^{(t)}}{\eta^{(t)}} \leq \frac{w^{(t-1)}}{\eta^{(t-1)}}$ as in the original proof, it is equivalent to have $(c-3)(a+t)^2 + 3(a+t) - 1 \geq 0$ for all t . It is thus sufficient to have $(c-3)(a+t)^2 + 3(a+t) - 1|_{t=0} = (c-3)a^2 + 3a - 1 \geq 0$ for a choice of $c > 3$, which is satisfied by, e.g., $c = 3.25$ and any parameter $a \geq \frac{13L}{\mu}$. (By definition, $L \geq \mu$ and thus $a \geq 13$.) Next, by letting $t = T-1$ and recursively applying

$$v_e^{(t+1)} \frac{w^{(t)}}{\eta^{(t)}} \leq \frac{w^{(t-1)}}{\eta^{(t-1)}} v_e^{(t)} + w^{(t)}A + w^{(t)}\eta^{(t)}B + w^{(t)}(\eta^{(t)})^2C - w^{(t)}f_e^{(t)}, \quad (78)$$

it follows that

$$\sum_{t=0}^{T-1} w^{(t)} f_e^{(t)} \leq (1 - \eta^{(0)} \mu) \frac{w^{(0)}}{\eta^{(0)}} v_e^{(0)} + \sum_{t=0}^{T-1} w^{(t)} A + \sum_{t=0}^{T-1} w^{(t)} \eta^{(t)} B + \sum_{t=0}^{T-1} w^{(t)} (\eta^{(t)})^2 C. \quad (79)$$

As a result, plugging $\eta^{(0)} = \frac{3.25}{\mu a}$ and dividing both sides of (79) by S_T , we obtain (76). \blacksquare

According to Lemma F.2, for constants $A = \frac{1}{K^2} \omega^2 d \frac{\mu}{3.25} (\zeta_0(\delta, \omega) a')^2 \sqrt{\tilde{N}_{0,T}}$, $B = \frac{\bar{\sigma}^2}{K}$ and $C = \frac{15L}{(p^{(T)}(\delta, \omega))^2} (24G^2 + \sqrt[4]{\tilde{N}_{0,T}} A(\delta, \omega)/K)$, as well as $f_e^{(t)} = \mathbb{E}[F(\bar{\theta}^{(t)})] - F^*$, (74) implies that

$$\begin{aligned} \frac{1}{S_T} \sum_{t=0}^{T-1} w^{(t)} \mathbb{E}[F(\bar{\theta}^{(t)})] - F^* &\leq \frac{\mu}{3.25} \frac{a^3 - 3.25a^2}{S_T} v_e^{(0)} + \frac{158.45 \left(24G^2 + \frac{A(\delta, \omega)}{K} \sqrt[4]{\tilde{N}_{0,T}} \right) LT}{\mu^2 (p^{(T)}(\delta, \omega))^2 S_T} + \\ &\quad \frac{1.625T(T+2a) \bar{\sigma}^2}{\mu S_T} \frac{1}{K} + \frac{1}{K^2} C(\delta, \omega) \sqrt{\tilde{N}_{0,T}}. \end{aligned} \quad (80)$$

Combined (80) with $F(\tilde{\theta}_T) = F(\frac{1}{S_T} \sum_{t=0}^{T-1} w^{(t)} \bar{\theta}^{(t)}) \leq \frac{1}{S_T} \sum_{t=0}^{T-1} w^{(t)} F(\bar{\theta}^{(t)})$, which is due to Jensen's inequality, Theorem 5.1 is thus proved.

REFERENCES

- [1] H. Xing, O. Simeone, and S. Bi, "Decentralized federated learning via SGD over wireless D2D networks," in *IEEE International Workshop on Signal Processing Advances in Wireless Communications (SPAWC)*, Atlanta, GA, USA, May 2020.
- [2] R. Bekkerman, M. Bilenko, and J. Langford, *Scaling up machine learning: Parallel and distributed approaches*. Cambridge Univ. Press, 2011.
- [3] T.-H. Chang, M. Hong, H.-T. Wai, X. Zhang, and S. Lu, "Distributed learning in the nonconvex world: from batch to streaming data, and beyond," *IEEE Signal Process. Mag.*, vol. 37, no. 3, pp. 26–38, May 2020.
- [4] P. Kairouz, H. B. McMahan *et al.*, "Advances and open problems in federated learning," *to appear in Foundations and Trends® in Machine Learning*, vol. 14, no. 1, Mar. 2021.
- [5] T. Li, A. K. Sahu, A. Talwalkar, and V. Smith, "Federated learning: Challenges, methods, and future directions," *IEEE Signal Process. Mag.*, vol. 37, no. 3, pp. 50–60, May 2020.
- [6] Z. Zhou, X. Chen, E. Li, L. Zeng, K. Luo, and J. Zhang, "Edge intelligence: Paving the last mile of artificial intelligence with edge computing," *Proc. IEEE*, vol. 107, no. 8, pp. 1738–1762, Jun. 2019.
- [7] G. Zhu, D. Liu, Y. Du, C. You, J. Zhang, and K. Huang, "Toward an intelligent edge: Wireless communication meets machine learning," *IEEE Commun. Mag.*, vol. 58, no. 1, pp. 19–25, Jan. 2020.
- [8] D. Alistarh, D. Grubic, J. Li, R. Tomioka, and M. Vojnovic, "QSGD: Communication-efficient SGD via gradient quantization and encoding," in *Advances in Neural Information Processing Systems (NeurIPS)*, Long Beach, CA, USA, Dec. 2017.
- [9] J. Bernstein, Y.-X. Wang, K. Azizzadenesheli, and A. Anandkumar, "signSGD: Compressed optimisation for non-convex problems," in *International Conference on Machine Learning (ICML)*, Stockholm, Sweden, Jul. 2018.
- [10] A. Abdi, Y. M. Saidutta, and F. Fekri, "Analog compression and communication for federated learning over wireless MAC," in *IEEE International Workshop on Signal Processing Advances in Wireless Communications (SPAWC)*, Atlanta, GA, USA, May 2020.

- [11] J. Wu, W. Huang, J. Huang, and T. Zhang, “Error compensated quantized SGD and its applications to large-scale distributed optimization,” in *International Conference on Machine Learning (ICML)*, Stockholm, Sweden, Jul. 2018.
- [12] D. Basu, D. Data, C. Karakus, and S. Diggavi, “Qsparse-local-SGD: Distributed SGD with quantization, sparsification and local computations,” in *Advances in Neural Information Processing Systems (NeurIPS)*, Vancouver, Canada, Dec. 2019.
- [13] M. M. Amiri and D. Gündüz, “Federated learning over wireless fading channels,” *IEEE Trans. Wireless Commun.*, vol. 19, no. 5, pp. 3546–3557, May 2020.
- [14] R. Xin, S. Kar, and U. A. Khan, “Decentralized stochastic optimization and machine learning: A unified variance-reduction framework for robust performance and fast convergence,” *IEEE Signal Process. Mag.*, vol. 37, no. 3, pp. 102–113, May 2020.
- [15] H. Xu, L. Zhang, E. Sun, and C.-L. I, “Be-ran: Blockchain-enabled RAN with decentralized identity management and privacy-preserving communication,” *arXiv preprint arXiv:2101.10856*, 2021.
- [16] E. Ozfatura, S. Rini, and D. Gunduz, “Decentralized SGD with over-the-air computation,” *arXiv preprint arXiv:2003.04216*, 2020.
- [17] A. Nedić, A. Olshevsky, and M. G. Rabbat, “Network topology and communication-computation tradeoffs in decentralized optimization,” *Proc. IEEE*, vol. 106, no. 5, pp. 953–976, Apr. 2018.
- [18] S. Savazzi, M. Nicoli, and V. Rampa, “Federated learning with cooperating devices: A consensus approach for massive IoT networks,” *IEEE Internet Things J.*, vol. 7, no. 5, pp. 4641–4654, May 2020.
- [19] R. Xin, S. Kar, and U. A. Khan, “An introduction to decentralized stochastic optimization with gradient tracking,” *arXiv preprint arXiv:1907.09648v2*, 2019.
- [20] H. Tang, X. Lian, M. Yan, C. Zhang, and J. Liu, “ D^2 : Decentralized training over decentralized data,” in *International Conference on Machine Learning (ICML)*, Stockholm, Sweden, Jul. 2018.
- [21] A. Koloskova, S. U. Stich, and M. Jaggi, “Decentralized stochastic optimization and gossip algorithms with compressed communication,” in *International Conference on Machine Learning (ICML)*, Long Beach, CA, USA, Jun. 2019.
- [22] A. Koloskova, T. Lin, S. U. Stich, and M. Jaggi, “Decentralized deep learning with arbitrary communication compression,” in *International Conference on Learning Representations (ICLR)*, Apr. 2020.
- [23] N. Singh, D. Data, J. George, and S. Diggavi, “SPARQ-SGD: Event-triggered and compressed communication in decentralized stochastic optimization,” in *IEEE Conference on Decision and Control (CDC)*, Jeju Island, Korea (South), Dec. 2020.
- [24] M. Chen, H. V. Poor, W. Saad, and S. Cui, “Wireless communications for collaborative federated learning,” *IEEE Commun. Mag.*, vol. 58, no. 12, pp. 48–54, Dec. 2020.
- [25] G. Zhu, Y. Wang, and K. Huang, “Broadband analog aggregation for low-latency federated edge learning,” *IEEE Trans. Wireless Commun.*, vol. 19, no. 1, pp. 491–506, Jan. 2020.
- [26] Q. Zeng, Y. Du, K. Huang, and K. K. Leung, “Energy-efficient radio resource allocation for federated edge learning,” in *IEEE International Conference on Communications Workshops (ICC Workshops)*, Dublin, Ireland, Jul. 2020.
- [27] M. Chen, Z. Yang, W. Saad, C. Yin, H. V. Poor, and S. Cui, “A joint learning and communications framework for federated learning over wireless networks,” *IEEE Trans. Wireless Commun.*, vol. 20, no. 1, pp. 269–283, Jan. 2021.
- [28] T. Nishio and R. Yonetani, “Client selection for federated learning with heterogeneous resources in mobile edge,” in *IEEE International Conference on Communications (ICC)*, Shanghai, China, May 2019.
- [29] J.-H. Ahn, O. Simeone, and J. Kang, “Wireless federated distillation for distributed edge learning with heterogeneous data,” in *IEEE International Symposium on Personal, Indoor and Mobile Radio Communications (PIMRC)*, Istanbul, Turkey, Sep. 2019.

- [30] W. Liu, X. Zang, Y. Li, and B. Vucetic, “Over-the-air computation systems: Optimization, analysis and scaling laws,” *IEEE Trans. Wireless Commun.*, vol. 19, no. 8, pp. 5488–5502, Aug. 2020.
- [31] H. Guo, A. Liu, and V. K. N. Lau, “Analog gradient aggregation for federated learning over wireless networks: Customized design and convergence analysis,” *IEEE Internet Things J.*, vol. 8, no. 1, pp. 197–210, Jan. 2021.
- [32] X. Wei and C. Shen, “Federated learning over noisy channels: Convergence analysis and design examples,” *arXiv preprint arXiv: 2101.02198*, 2021.
- [33] J. Wang, A. K. Sahu, Z. Yang, G. Joshi, and S. Kar, “MATCHA: Speeding up decentralized SGD via matching decomposition sampling,” in *Indian Control Conference*, Hyderabad, India, Dec. 2019.
- [34] L. Xiao and S. Boyd, “Fast linear iterations for distributed averaging,” *Systems & Control Letters*, vol. 53, no. 1, pp. 65–78, Sept. 2004.
- [35] H. Xiao, K. Rasul, and R. Vollgraf, “Fashion-MNIST: a novel image dataset for benchmarking machine learning algorithms,” *arXiv preprint arXiv:1708.07747*, 2017.
- [36] T. Husfeldt, “Graph colouring algorithms,” 2015.
- [37] N. J. Higham, *Accuracy and stability of numerical algorithms*. Philadelphia, PA, USA: SIAM, 2002.
- [38] S. U. Stich, J.-B. Cordonnier, and M. Jaggi, “Sparsified SGD with memory,” in *Advances in Neural Information Processing Systems (NeurIPS)*, Montreal, Canada, Dec. 2018.